RSC Advances

REVIEW

View Article Online
View Journal | View Issue

Cite this: *RSC Adv.*, 2026, **16**, 1643

Upconversion materials: a new frontier in solar water-splitting

Yerbolat Magazov,[ab] Asset Aliyev,[ab] Nursaya Zhumabay,[ab] Zhamilya Taubaldiyeva,[c] Guldana Zhigerbayeva *[ab] and Nurxat Nuraje *[abcd]

Limited utilization of the solar spectrum is a major bottleneck in photocatalytic water-splitting, as most semiconductor photocatalysts only harness UV or visible light, leaving a large fraction of infrared photons unused. Upconversion materials have emerged as a promising solution by converting two or more low-energy photons into a single higher-energy photon, thereby extending the photoresponse of water-splitting systems. This review provides a technical overview of the two leading upconversion strategies for solar hydrogen generation: lanthanide (Ln)-based upconversion phosphors and triplet–triplet annihilation (TTA) upconversion systems, including purely organic and metal–organic approaches. We discuss how Ln-doped upconverters can enable near-infrared-driven photocatalysis, while highlighting their efficiency limitations under 1-sun illumination. We then examine TTA-based upconversion, which leverages molecular sensitizer–emitter pairs to achieve efficient upconversion under solar light intensities, and summarize recent demonstrations of TTA systems boosting H_2 production and even enabling overall water splitting under visible light. A comparative analysis of Ln-based *vs.* TTA-based systems is presented, underscoring their respective advantages (spectral range, stability, efficiency) and constraints. Finally, we outline future research directions and integration strategies aimed at combining the strengths of both upconversion approaches to maximize solar-to-hydrogen efficiency. The insights from this review suggest that upconversion materials can play a complementary and transformative role in next-generation solar water-splitting technologies.

Received 27th September 2025
Accepted 22nd December 2025

DOI: 10.1039/d5ra07342a

rsc.li/rsc-advances

1. Introduction

Solar water-splitting is one of the ideal routes to get green hydrogen.[1–5] Despite thorough research[6–8] conducted over several decades, there are still various obstacles in the field of materials science that need to be addressed to recognize solar water-splitting as a viable and inexpensive method for H_2 generation. Oxide-based photocatalysts have garnered significant interest as an economically feasible alternative. This is primarily owing to their plentiful elemental availability and the ability to synthesize them on a large scale.[9] Extensive research was conducted to enhance the produced photocurrent and durability of the water-splitting system by exploring heterojunction partners,[10–12] solid-state overlayers,[13] and catalytic interfaces.[14–16] However, the restricted effectiveness in harnessing solar energy continues to impede photocatalysis, mainly because photocatalysts generally have a narrow absorption spectrum. Efforts were made to enhance the effectiveness of light harnessing by enhancing the crystallinity or regulating the surface topology.[17–21] However, most semiconductor photocatalysts (TiO_2, $SrTiO_3$) are only activated by ultraviolet (UV) or a portion of visible light, meaning a large portion of the solar spectrum – particularly the infrared (IR) region – is wasted. For instance, UV photons constitute only 9% of sunlight, while visible light contributes 54%, and the remaining 37% is IR.[22] Photons beyond the bandgap of the catalyst pass through without generating any reaction. This spectral mismatch severely limits the solar-to-hydrogen conversion efficiency in practical systems. Improving light harvesting beyond the UV-visible range is therefore a critical challenge for solar water-splitting technologies.

One emerging strategy to overcome this limitation is the implementation of photon upconversion materials into photocatalytic systems. Photon upconversion (UC) is the process by which two or more low-energy photons are combined to produce one higher-energy photon.[23] By placing upconversion materials in or near a photocatalyst, sub-bandgap photons that would normally be lost (*e.g.*, red or IR light that a wide-bandgap catalyst cannot absorb) can be transformed into photons of sufficiently high energy to drive water-splitting reactions. In essence, upconverters act as spectral converters that open up additional portions of the solar spectrum for photocatalysis.

[a]*Renewable Energy Lab, National Laboratory Astana, Astana, 010000, Kazakhstan. E-mail: guldana.zhigerbaeva@nu.edu.kz; nurxat.nuraje@nu.edu.kz*

[b]*Institute of New Materials and Energy Technologies, Astana, 010000, Kazakhstan*

[c]*Department of Chemical and Materials Engineering, Nazarbayev University, Astana, 010000, Kazakhstan*

[d]*Teqnovate LLC, Astana, 010000, Kazakhstan*

Among the various upconversion mechanisms, two have garnered particular interest for solar fuel applications: (1) lanthanide (Ln)-doped upconversion phosphors, and (2) triplet–triplet annihilation (TTA) upconversion systems. Notably, recent studies have identified TTA-based upconversion as especially effective under 1-sun solar illumination (owing to its high efficiency at low excitation power), whereas achieving efficient upconversion with Ln^{3+} ions under unconcentrated sunlight is considerably more challenging. This has motivated parallel research into both approaches, as each offers distinct strengths for extending solar light harvesting.

Lanthanide-based upconversion materials typically consist of an inorganic host crystal doped with trivalent lanthanide ions (such as Er^{3+}, Tm^{3+}, or Ho^{3+} sensitized by Yb^{3+}).[24] These ions can absorb two or more infrared photons through stepwise f–f electronic excitations and emit a higher-energy photon *via* radiative relaxation (the Anti-Stokes upconversion process). The rugged inorganic nature of Ln-doped upconverters ($NaYF_4$:Yb/Er nanophosphors) makes them chemically stable and compatible with harsh photocatalytic environments.[25] Moreover, they offer the unique advantage of accessing deep-IR wavelengths beyond the absorption range of typical semiconductors. Indeed, coupling lanthanide upconversion phosphors to photocatalysts has enabled NIR-driven hydrogen generation in proof-of-concept studies. For example, Er^{3+}/Yb^{3+}-doped phosphors have been used to upconvert 980 nm light (near-IR) into UV/visible output sufficient to drive H_2 evolution in the presence of sacrificial reagents.[26] Despite such promising demonstrations, Ln-based upconversion faces significant limitations. NIR photons carry lower energy and are more weakly absorbed. In fact, the notion of harvesting the NIR portion of sunlight for photocatalysis has been met with some skepticism, partly because water itself absorbs in the near-IR, and partly because of the inherently low quantum yield of lanthanide upconversion processes.

In parallel, triplet–triplet annihilation upconversion (TTA-UC) has emerged as an attractive alternative approach, especially suited for lower-intensity excitation conditions.[27] TTA-based upconversion is a photochemical process typically involving organic or organometallic chromophores in solution or polymeric matrices. In a canonical TTA system, a sensitizer molecule absorbs a low-energy photon and populates a long-lived triplet excited state. This triplet energy is then transferred to an emitter molecule, raising it to an excited triplet state. When two such excited emitter molecules encounter one another, they can undergo triplet–triplet annihilation, wherein one molecule relaxes and transfers its energy to the other, promoting the latter to a higher-energy singlet excited state that emits an upconverted photon (usually in the UV or blue range).[26–28] A key distinction of TTA-UC is that it does not require high photon flux. Many TTA systems can achieve efficient upconversion (with upconversion quantum yields on the order of tens of percent) under non-coherent, 1-sun solar illumination. This makes TTA mechanisms highly relevant for solar water splitting. Nonetheless, TTA systems come with their own challenges. The organic emitter and sensitizer molecules can be prone to photobleaching or chemical degradation, especially under UV exposure. Moreover, TTA upconversion typically requires deoxygenated conditions because molecular oxygen effectively quenches the crucial triplet states. In practice, current TTA upconverters for water splitting have exhibited limited operational stability – for instance, the TTA-UC solution used in one prototype showed a useful upconversion lifetime on the order of only 10 minutes before degrading. Developing more stable, oxygen-tolerant TTA systems (through improved molecular design or encapsulation in protective matrices) is therefore an active area of research.[26]

Several recent reviews have discussed upconversion materials or triplet–triplet annihilation (TTA) concepts within broader frameworks of near-infrared (NIR)-responsive photocatalysis,[29–35] heterojunction/Z-scheme design,[36] or material-specific advances in TiO_2 (ref. 37 and 38) and g-C_3N_4.[39] In these articles, upconversion-assisted water splitting is typically treated as a short subsection, often illustrated by a limited number of model systems (most commonly TiO_2- and g-C_3N_4-based composites) rather than offering a comprehensive, water-splitting-centered assessment across diverse semiconductor platforms. Moreover, even when "water splitting and upconversion" are mentioned, the concept is frequently demonstrated using dye-degradation model reactions rather than a focused evaluation of genuine H_2 evolution or overall water splitting performance. A dedicated overview focused specifically on upconversion-assisted photocatalytic and photoelectrochemical water splitting remains scarce, with an earlier mini-review from Fan *et al.*[40] (2014), providing only a brief snapshot of the field. Collectively, these gaps indicate the need for an updated and specialized synthesis that consolidates recent progress, clarifies structure–function relationships, and provides practical design guidance for implementing upconversion in modern solar water-splitting architectures.

In the following sections, we review and compare the roles of lanthanide-based and TTA-based upconversion materials in advancing solar water-splitting. First, we discuss Ln-doped upconversion nanomaterials and their integration into photocatalytic systems, highlighting recent progress in enhancing NIR photon utilization. Next, we examine organic and metal–organic TTA upconversion systems for photocatalysis, including their working principles and key demonstrations in solar hydrogen production. In the following section, we present a comparative analysis of the two upconversion strategies, critically evaluating their advantages, limitations, and the ways in which they can complement each other to maximize solar spectrum usage. Finally, we outline future directions for research and development, emphasizing material improvements and integration strategies needed to translate upconversion-augmented water-splitting from laboratory studies to efficient, scalable solar fuel devices.

2. The use of Ln-based compounds in photocatalytic systems

UC differs from other multiphoton absorption processes by the involvement of real intermediate electronic states as opposed to

virtual states. The long-lived nature of these states (micro- to milliseconds) allows sufficient population buildup, increasing the probability that subsequent photons are absorbed before non-radiative relaxation occurs.[41]

Such intermediate states are found in transition metals and especially in trivalent lanthanide ions (Ln^{3+}).[42,43] In lanthanides, this is possible due to 4f-to-4f transitions, which are parity forbidden and therefore result in low oscillator strength and long lifetimes. However, when symmetry is broken, the f states of Ln^{3+} ions interact with other states of opposite parity, forming mixed-parity states, between which these transitions become partially allowed.[44–46] In addition, shielding of the f orbital results in weak electron–phonon coupling, which prevents electrons from losing their energy due to the lattice effect, thereby increasing their lifetime.[41]

The host lattice plays a decisive role in governing upconversion efficiency. A lower degree of symmetry generally prolongs the lifetime of excited states and increases the probability of optical transitions. Therefore, tuning the crystal symmetry of the host lattice is a key strategy to enhance upconversion luminescence (UCL). Additionally, the crystal-field strength imposed by the surrounding lattice influences the energy levels of Ln^{3+} ions, thereby affecting transition probabilities and emission characteristics.[47,48] Equally important, the host lattice should possess low phonon energies to minimize nonradiative multiphoton relaxation. In fact, phonon energy is often considered an even more critical factor for UCL efficiency than lattice symmetry.[41]

Several photophysical processes contribute to upconversion (UC), including ground-state absorption (GSA), excited-state absorption (ESA), energy transfer (ET), and energy migration (EM). The ion responsible for emitting UCL is referred to as the activator. Its efficiency can be significantly enhanced by coupling it with sensitizer ions, which efficiently absorb incident light and transfer the harvested energy to the activator, thereby boosting the overall UC process. Depending on the type and number of active centers involved, upconversion (UC) can proceed *via* three principal mechanisms: GSA/ESA, GSA/ETU, and GSA/EMU.

The GSA/ESA mechanism is the simplest, requiring only a single active ion.[41] In this case, an electron sequentially undergoes ground-state absorption (GSA) and excited-state absorption (ESA), which ultimately leads to upconversion luminescence (UCL).

In the GSA/ETU mechanism, two active centers participate. These may be either two identical activator ions or a sensitizer–activator pair. In the first scenario, both activators absorb photons, and the excitation energy is transferred to one ion, where UCL occurs. In the second case, the sensitizer absorbs photons and passes the energy to the activator, which then emits UCL.[41,49,50]

The GSA/EMU mechanism is more complex, potentially involving up to four distinct centers: sensitizer, accumulator, migrator, and activator. Here, the excitation energy is absorbed, stored, and transported across these centers before reaching the activator. Spatially distributing these roles within a core–shell architecture can minimize energy loss *via* cross-relaxation. This design also relaxes the requirements on the activator, such as the need for long excited-state lifetimes and intermediate energy levels.[41]

A schematic illustration and a comparative summary of these mechanisms are provided in Fig. 1 and Table 1, respectively.

Other, less common UC processes include cooperative sensitization (CSU), in which two sensitizers simultaneously transfer their energy to a single activator,[51] and a photon avalanche (PA), which relies on a feedback loop of ESA and cross-relaxation, leading to a sharp increase in UCL above a certain excitation threshold.[52]

Research into UC-based photocatalysis has evolved from early demonstrations using UCNP powders for dye degradation to more sophisticated thin-film and core–shell architectures designed for water splitting. The following sections review key strategies that have been employed to improve UC efficiency, with emphasis on host selection, nanostructure design, and integration with semiconductors.

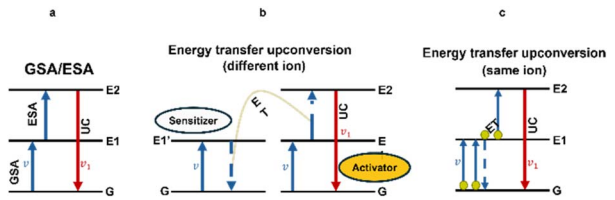

Fig. 1 Schematics of the main upconversion mechanisms: (a) GSA/ESA, (b) GSA/ETU and (c) GSA/EMU.

Table 1 Upconversion mechanisms

Mechanism	Description	Active centers	Key features
GSA/ESA	Single ion absorbs two photons sequentially (GSA → ESA)	1 (activator only)	Simple mechanism; low probability; strong power dependence
ETU (energy transfer upconversion)	Energy absorbed by one ion is transferred to another ion (activator or sensitizer–activator pair)	2 (or more)	Most common in lanthanide UC; efficient due to sensitizers
EMU (energy migration-mediated UC)	Energy migrates through a network of ions before reaching the activator	3–4 (sensitizer, migrator, activator, accumulator)	Enables core–shell designs; reduces cross-relaxation losses

While the general UC mechanisms (GSA/ESA, ETU, EMU) apply across Ln^{3+} systems, individual lanthanide ions display distinct spectroscopic features that strongly influence their upconversion behavior. For instance, Er^{3+} and Tm^{3+} possess ladder-like 4f energy manifolds that support efficient green-red and blue-UV UC emission, respectively, whereas Ho^{3+} typically yields green-yellow emission through well-defined ETU pathways.[53] Cerium-containing hosts behave quite differently. Ce^{3+}, with its single 4f electron, engages in parity-allowed 5d–4f transitions, leading to intense absorption but also enhanced electron–phonon coupling and faster nonradiative relaxation.[54] Moreover, cerium is one of the few lanthanides that readily cycles between +3 and +4 oxidation states. The coexistence of Ce^{3+}/Ce^{4+} can introduce defect levels, alter local charge-compensation environments, and modify the crystal field experienced by co-dopants such as Ho^{3+}, ultimately affecting UC efficiency either positively or negatively depending on the Ce^{3+}/Ce^{4+} ratio.[55] These ion-specific differences underscore the importance of understanding the electronic structure of each lanthanide when designing efficient UC photocatalysts.

Taken together, these upconversion pathways illustrate how lanthanide ions can harvest low-energy NIR photons and convert them into the UV-visible photons required to excite wide-bandgap semiconductors. By enabling access to a much larger portion of the solar spectrum and supplying additional excitation pathways, UC materials can therefore enhance light absorption, carrier generation, and overall photocatalytic performance in water-splitting systems.

2.1 Evolution of UC-based photocatalysis: from dye degradation to advanced architectures

In the early 2010s, the application of UC materials was predominantly directed toward photocatalytic dye degradation, typically employing simple physical mixtures or composite structures of UC nanoparticles with semiconductors such as ZnO and TiO_2.[56–60] Er^{3+} was among the first activators explored in these systems, followed later by more complex sensitizer–activator pairs such as Yb^{3+}–Er^{3+} and Yb^{3+}–Tm^{3+} embedded in host lattices like Y_3AlO_3 or YF_3. Photocatalytic performance was commonly assessed by monitoring the degradation of organic dyes, including acid red B and azo fuchsine. Photocatalytic performance was typically quantified from UV-vis absorption spectra and adsorption (eqn (1)) and degradation ratios (eqn (2)).

$$\text{Adsorption ratio (\%)} = [(C_0 - C_a)/C_0] \times 100 \quad (1)$$

$$\text{Absolute degradation ratio (\%)} = [(C_0 - C_t)/C_0] \times 100 \quad (2)$$

where C_0 is the initial dye concentration, C_a is the dye concentration after adsorption, and C_t is the concentration after solar light irradiation. Beyond endpoint degradation ratios, several studies also analyzed the time dependence of dye degradation, fitting the data to pseudo-first-order kinetics. This allowed the extraction of apparent rate constants, providing a more rigorous measure of photocatalytic efficiency and enabling comparisons across different materials and experimental conditions. For instance, Wang *et al.*[61] reported that the apparent rate constant increased from 0.2912 h^{-1} for β-$NaYF_4$:Yb, Er@SiO_2@TiO_2 to 0.3624 h^{-1} for β-$NaYF_4$:Yb, Tm@SiO_2@TiO_2, despite the Er^{3+} system exhibiting stronger UC luminescence. This result highlighted that the emission band position of the activator ion could be more decisive for photocatalytic activity than overall luminescence intensity, marking one of the first systematic comparisons of Er^{3+} and Tm^{3+} activators in UC photocatalysis.

The first decisive proof-of-concept for lanthanide upconversion enabling NIR-driven photocatalysis was reported in 2010, when YF_3:Yb,Tm/TiO_2 core–shell nanoparticles were shown to degrade dyes under NIR excitation.[58] This validated the concept of exploiting upconversion to activate wide-bandgap semiconductors beyond their intrinsic absorption range. While early demonstrations often relied on solar or simulated sunlight, subsequent studies increasingly adopted monochromatic 980 nm laser irradiation resonant with Yb^{3+} absorption, providing unambiguous evidence that photocatalytic activity originated from NIR-driven upconversion rather than direct UV excitation.[62–64]

In these studies, the concentration of Tm^{3+} was generally kept low (0.2–0.5 mol%) to avoid luminescence quenching, since, in principle, higher activator loading should increase UC emission but, in practice, often led to nonradiative losses. An important step in UC exploration came when Zhao *et al.*[65] demonstrated that this trade-off could be mitigated: under higher excitation intensities, efficient UC luminescence was achieved even at 8 mol% Tm^{3+} doping.[61] This was attributed to the enhanced population of excited states in both sensitizer and activator ions, with the upconversion luminescence intensity increasing by factors of 5.6, 71, and 1105 at 0.5, 4, and 8 mol% Tm^{3+}, respectively, under high irradiance. This finding was significant because it showed that the long-assumed constraint of concentration quenching was not absolute, opening new possibilities for designing UC materials with higher activator content.

During the same period, core–shell architectures gained traction as a strategy to suppress nonradiative losses and enhance interfacial charge transfer. In UC-semiconductor composites, two primary mechanisms contribute to energy transfer: Förster resonance energy transfer (FRET) and radiation reabsorption. Guo *et al.*[62] compared physical mixtures with composite core–shell structures and found that the latter induced stronger reductions in Tm^{3+} excited-state lifetimes, consistent with efficient FRET providing a direct, near-field energy transfer pathway. By contrast, radiation reabsorption-dominant in simple mixtures relies on emitted UC photons being reabsorbed by the semiconductor, a process that is inherently less efficient due to scattering and nonradiative losses. As a result, dye degradation reached 65% with UC-ZnO composites compared to only 35% for the mixture. By 2013, work on $NaYF_4$:Yb, Tm@TiO_2 (ref. 62) and related composites[64] further consolidated this principle, demonstrating that rational nanostructure design was critical to boosting UC-assisted photocatalysis.

Building on these advances, more recent efforts have shifted toward rational interface engineering. For example,

$NaYF_4$:Yb,Tm nanocrystals were selectively deposited on distinct BiOCl facets, revealing that the (110) facet, owing to its narrower bandgap and shorter hole diffusion length, enabled more efficient UC-driven photocatalysis than the (001) facet.[66] At the same time, the scope of photocatalytic applications has broadened. Whereas earlier demonstrations relied almost exclusively on model organic dyes, more recent reports tested the degradation of pharmaceutical contaminants such as ciprofloxacin and norfloxacin,[67,68] reflecting a shift toward evaluating UC photocatalysts under more realistic and environmentally relevant conditions. This expansion of target pollutants underscores the field's progression from conceptual validation to practical applicability. A summary of representative studies on dye degradation applications is provided in Table 2.

2.2 Synthesis strategies for Ln-based upconversion materials in photocatalytic water-splitting

Across recent literature, hydrothermal and wet-chemical methods remain the predominant approaches for synthesizing Ln-based upconversion (UC) materials for photocatalytic water-splitting. For instance, β-$NaYF_4$:Yb^{3+}/Tm^{3+} microdisks have been prepared *via* citrate-assisted hydrothermal treatment at 180 °C, enabling straightforward *in situ* growth of Ag_3PO_4/Ag nanoparticles and subsequent assembly of g-C_3N_4 nanosheets to form hierarchical UC-semiconductor hybrids.[58] Hydrothermal and solvothermal methods are also pivotal in fabricating UC@semiconductor composites, as illustrated by O'Callaghan *et al.*,[70] who prepared UC/TiO_2 thin films for PEC devices by deposition of TiO_2 shells onto β-$NaYF_4$:Yb^{3+},Tm^{3+} *via* solvothermal coating. Complementary wet-chemical approaches such as polyol-mediated solvothermal synthesis have also been demonstrated.[66] Thus, morphology and UC intensity were modulated simply through precursor concentration in CeF_3:Ho^{3+} nanoparticles, directly influencing photocatalytic activity upon coupling with TiO_2. Meanwhile, template-assisted dip-coating allows for the preparation of ordered UC-oxide architectures, such as WO_3:Yb,Er inverse-opal structures, fabricated by Ma *et al.*[71] This was followed by *in situ* growth of $Zn_{0.5}Cd_{0.5}S$ nanoparticles to create efficient NIR-responsive heterojunctions. Aside from that, oxide-based UC hosts such as $Bi_3Ti_2O_8F$:Yb^{3+},Er^{3+} have been obtained by conventional high-temperature solid-state reactions, demonstrating that UC doping can also be integrated directly into semiconductor lattices.[52] Solvothermal core–shell $NaYF_4$ UC nanoparticles remain another important class, not only for forming heterostructures but also as free-floating UC additives in PEC systems, as reported by Feng *et al.*,[72] who used oleic-acid-derived core–shell–shell UCNPs dispersed in the electrolyte to extend photoresponse into the NIR. Finally, hydrothermal assembly is frequently employed to couple solvothermally synthesized UCNPs with semiconductors, as in Gao *et al.*,[73] where $NaYF_4$:Yb/Er nanoparticles were integrated with CdS and reduced graphene oxide in a single hydrothermal step to create a ternary photocatalyst with enhanced charge transport and broadened absorption. Altogether, these studies demonstrate that although hydrothermal and solvothermal routes dominate the preparation of UC materials, complementary methods play important roles in tailoring the structure, interfacial contact, and ultimately, photocatalytic water-splitting performance.

2.3 Beyond dyes: core–shell *vs.* powder structures for H_2 generation

This diversification of applications highlights how Ln-based UC research matured from proof-of-concept dye degradation toward more practical photocatalytic challenges. Building on this foundation, researchers soon extended UC-assisted photocatalysis to hydrogen generation. Efforts to optimize UC systems for solar fuels have diversified along several complementary directions, reflecting the different requirements of powder-based suspensions *versus* thin-film devices. For example, Feng *et al.*[72] employed an inert $NaYF_4$ shell to passivate UCNPs, thereby suppressing surface quenching, and achieved notable photocatalytic performance, with 16 μmol of H_2 generated within 3 h and photocurrent densities reaching −4 mA cm^{-2}. Around the same time, increasingly sophisticated Ln-based architectures were reported. For instance, Lee *et al.*[74] achieved photocurrent densities of 1.4 μA cm^{-2}, Gao *et al.*[73] demonstrated 301 μA cm^{-2} with concomitant hydrogen production of 2799 μmol h^{-1} g^{-1}, and Murali *et al.*[75] fabricated a novel $NaYF_4$:Yb/Tm@Ag_3PO_4/Ag@g-C_3N_4 architecture that achieved hydrogen production of 23.56 mmol g^{-1} h^{-1}.

By contrast, in 2024, O'Callaghan *et al.*[70] demonstrated that in thin-film configurations, simple mixtures of UC particles with semiconductors outperformed directly coated architectures, underscoring that the optimal design strategy depends strongly on the system geometry. They reported that mixtures of UC particles with semiconductors generated a significantly higher photocurrent (0.08 μA) than directly coated core–shell systems (0.03 μA). This enhancement was attributed to more efficient electron transport through the electrode, uniform illumination of the TiO_2 film, and improved connectivity between semiconductor particles, the ITO substrate, and the electrolyte. Their analysis further suggested that while core–shell designs are advantageous for colloidal suspensions, spatially separated mixtures are better suited for thin-film electrodes, offering benefits such as reduced nonradiative de-excitation, greater local particle concentration in the illuminated region, and the potential for reusability. Importantly, these results highlighted that design strategies must be tailored to the system architecture, as approaches beneficial in one configuration may hinder performance in another.

Another particularly notable recent advance was reported by Ma *et al.*[71] in 2024, who proposed a dual-functional upconversion strategy in which a single sensitizer simultaneously contributes photon–photon and photo-electronic processes. In this design, WO_3:Yb,Er not only converts NIR photons into visible light through the conventional Yb^{3+} → Er^{3+} upconversion pathway but also contributes to charge generation by transferring excited electrons directly into the semiconductor photocatalyst. Coupling this dual-action sensitizer with $Zn_{0.5}Cd_{0.5}S$ enabled a hydrogen evolution rate of 24.3 mmol g^{-1}

Table 2 Representative studies on the application of dye degradation

Year	UC material and paired semiconductor	Architecture type	Excitation	Dye model	Degradation rate	Other performance metrics	Ref.
2009	Er^{3+}:Y_3AlO_3/ZnO	Powder mixture	Solar light	Acid red B	60 min irradiation: 85.48% pure ZnO: 68.11%	Reaction rate constants (pseudo-first order): 0.0396 min^{-1} pure ZnO: 0.0190 min^{-1}	Wang *et al.*[56]
2010	Er^{3+}:Y_3AlO_3/Fe and Co-doped TiO_2	Powder mixture	Solar light	Azo fuchsine	Fe-doped: 97.92% Co-doped: 96.15%	Reaction rate constants (pseudo-first order): Fe-doped: 0.0750 min^{-1} Co-doped: 0.0549 min^{-1} (25% Er^{3+}:$YAlO_3$ content)	Xu *et al.*[57]
2010	YF_3:Yb^{3+}, Tm^{3+}/TiO_2	Core–shell/nanoparticles (powder)	980 nm laser and NIR (>700 nm)	Methylene blue	30 h irradiation: 61%	—	Qin *et al.*[58]
2013	β-$NaYF_4$:Yb^{3+},Tm^{3+} @ZnO	Core–shell *vs.* physical mixture (both in powder form)	980 nm laser	Rhodamine B	30 h irradiation 65% core–shell 35% mixture	Composites exhibited a significantly faster and higher generation of hydroxyl radicals ($OH^{\bullet}$) compared to the mixture	Guo *et al.*[62]
2013	β-$NaYF_4$:$Y^{3+}Tm^{3+}$/ Er^{3+}@Si@TiO_2	Double-shell-structure	980 nm laser	Rhodamine B	—	Reaction rate constants (first order): increased from 0.2912 h^{-1} (k(Er)) to 0.3624 h^{-1} (k(Tm))	Wang *et al.*[61]
2016	$NaYF_4$:Yb,Tm@BiOCl	Nanocrystals attached to nanoplates (powder)	980 nm laser	Rhodamine B	7.63×10^{-3} g RhB per g cat per h	TOC (total organic carbon) analysis: mineralization degree is 52% after 72 h	Bai *et al.*[66]
2019	N-doped TiO_2/(Ca,Y)F_2:Yb^{3+}, Tm^{3+}	Spindle-like nanoporous structure	980 nm laser	Methyl orange	65.6% degraded for 10 h	Pseudo-first-order kinetics: 0.05233 h^{-1}	Wang *et al.*[69]
2025	Er^{3+}/Yb^{3+} codoped@$BaCO_3$–Ta_2O_5–Bi_2O_3–SiO_2	Glass-ceramic/perovskite/ $BiCl_3O_{12}$ nanosheets	980 nm laser	Norfloxacin	For 150 min irradiation: 60%	—	Homg *et al.*[68]
2025	Yb^{3+}, Er^{3+}@$Bi_3Ti_2O_8F$	Nanoplates	980 nm laser	Ciprofloxacin	—	Reaction rate constant: plain BTOF: 0.00023 h^{-1} With Er^{3+}: 0.00178 h^{-1} Er^{3+}&Yb^{3+}: 0.00808 h^{-1}	Li *et al.*[67]

Table 3 Hydrogen evolution (solar water-splitting) under NIR

Year	UC material	Paired semiconductor	Architecture type	Excitation	Performance metrics	Ref.
2012	$NaYF_4$:Yb,Er (REN – rare earth nanocrystals)	Hematite	Composite films (slurry casted on hematite thin film)	980 nm laser	0.15 μA cm^{-2} current density	Zhang *et al.*[79]
2013	Er^{3+}/Yb^{3+} co-doped $NaYF_4$	ZnO nanorods decorated with CdTe QDs	Thin films (ZnO nanorods on FTO)	980 nm laser	0.045 μmol h^{-1} of H_2 produced	Chen *et al.*[80]
2020	$NaYF_4$@-$NaYbF_4$:Tm1% @$NaYF_4$, $NaYF_4$:Yb20%/Er2% @$NaYF_4$, and $NaYbF_4$:Er60% @$NaYF_4$	Cu_2ZnSnS_4	Core–shell and core–shell–shell structures	980 nm laser	Hydrogen production: 16 μmol within 3 h Photocurrent density: −4 mA cm^{-2}	Feng *et al.*[72]
2020	(Yb,Er) and (Yb,Tm)-doped YF_3 on oxyfluoride glass-ceramics	CdSe/ZnO	CdSe QDs/ZnO NRs fabricated on Tm and Er substrates on ITO	980 nm laser	Photocurrent densities 0.65 μA cm^{-2} and 1.4 μA cm^{-2} for Er and Tm, respectively	Lee *et al.*[74]
2021	β-$NaYF_4$:Yb^{3+}/Tm^{3+}	@Ag_3PO_4/Ag@g-C_3N_4	Ag_3PO_4/Ag nanoparticles and g-C_3N_4 nanosheets on UC $NaYF_4$:Yb/Tm hexagonal disks	λ > 400 nm	23.56 mmol g^{-1} h^{-1} hydrogen produced photocurrent: $NaYF_4$:Yb/Tm@Ag_3PO_4/Ag@g-C_3N_4 2 times as high as $NaYF_4$:Yb/Tm@Ag_3PO_4/Ag	Murali *et al.*[75]
2022	$NaYF_4$:Yb^{3+}, Tm^{3+} (NYF)	d g-C_3N_4 (DCN)	NYF nanocrystals on DCN nanocloumns/on FTO	Solar light	Current density: 301 μA cm^{-2} hydrogen production: 2799 μmol h^{-1} g^{-1}	Gao *et al.*[73]
				980 nm laser	Photocurrent: 8.01 μA 1251 μmol h^{-1} g^{-1}	
2024	$NaYF_4$:Yb, Tm^{3+}	TiO_2	Core shell *vs.* mixtures on ITO foils	980 nm laser	0.08 μA (mixture) and 0.03 μA (shell structure)	O'Callaghan[70]
2024	WO_3:Yb, Er	$Zn_{0.5}Cd_{0.5}S$	Core–shell structure	NIR and solar light pre-treatment	24 mmol g^{-1} h^{-1} of H_2 produced and 41 mmol g^{-1} h^{-1} with Ni_2P co-catalyst	Ma *et al.*[71]
2024	Yb^{3+}–Er^{3+}–Tm^{3+}	TiO_2/ZBLAN (ZrF_4–BaF_2–LaF_3–AlF_3–NaF)	Photoelectrode + ZBLAN glass	980 nm laser (340–410 nm to activate TiO_2)	Photoanodic current of 3.5–4 μA cm^{-2}	Méndez-Ramos *et al.*[76]
2025	30% Ho^{3+}	CeF_3/TiO_2	UC/semiconductor nanosystem	λ > 400 nm	2203 μmol H_2 per g of catalyst	Verma *et al.*[81]

h^{-1} under simulated solar light without any cocatalyst. Upon loading Ni_2P, the performance increased to 41.3 mmol g^{-1} h^{-1} at 10 °C and further reached 93.3 mmol g^{-1} h^{-1} under non-temperature-controlled conditions. By simultaneously enhancing both photon utilization and charge transfer, this approach significantly improved overall system efficiency, positioning dual-functional UC strategies as a promising direction for high-performance solar hydrogen generation.

2.4 Glassy matrices as scalable hosts for Ln-based upconversion

A consistent theme in the work of Méndez-Ramos[76,77] and collaborators have been exploring glassy matrices as alternative hosts for rare-earth-doped upconversion systems. Early efforts centered on oxyfluoride nano-glass-ceramics, where low-phonon fluoride nanocrystals (PbF_2, $NaYF_4$, YF_3, KYF_4) were dispersed within silica matrices to achieve strong UV-blue upconversion luminescence, thereby extending the absorption window of water-splitting semiconductors. More recently, the group has advanced to fluoride glass matrices of the ZBLAN family (ZrF_4–BaF_2–LaF_3–AlF_3–NaF), doped with Yb^{3+}, Er^{3+}, and Tm^{3+}, which demonstrated efficient NIR-to-UV/visible conversion and were successfully integrated into PEC devices as spectral converters. In these studies, the glass-based electrodes generated stable photo-anodic currents of 3.5–4 μA cm^{-2}, highlighting that glassy hosts can sustain not only strong UC luminescence but also measurable photocatalytic activity under operational conditions.

The broader promise of glassy hosts is also reflected in the work of Lee *et al.*,[74] mentioned above, who developed an oxyfluoride glass-ceramic platform decorated with functional nanostructures. Their design combined CdSe quantum dots on ZnO nanorods, integrated onto glass substrates doped with Er^{3+} or Tm^{3+}, supported on ITO. This multilayered architecture leveraged the strong UC luminescence of oxyfluoride glass-ceramics while coupling it with semiconductor nanostructures for charge generation and collection. Photocurrent densities of 0.65 μA cm^{-2} for Er-doped and 1.4 μA cm^{-2} for Tm-doped systems were reported, confirming that the choice of activator strongly impacts device performance. The result was a hybrid electrode that bridged photonic conversion with efficient charge separation, further validating glass-ceramics as flexible scaffolds for UC-semiconductor integration.

Importantly, Méndez-Ramos consistently positions glassy matrices against the benchmark crystalline host $NaYF_4$, long considered the most efficient UC medium due to its low phonon energy. While crystalline hosts deliver high luminescence yields, their drawbacks-limited processability, mechanical fragility, and challenges in device integration-restrict broader applications. By contrast, glassy hosts combine the optical merits of fluoride crystals with the transparency, robustness, and compositional flexibility of glass, enabling higher rare-earth solubility, large-area fabrication, and easier incorporation into device architectures. Complementary reports[78] further emphasize that, unlike conventional nanoparticle photocatalysts, which often suffer from agglomeration, poor recovery, and limited recyclability, glass-ceramics provide excellent luminescent properties, straightforward synthesis routes, and lower production costs.

Taken together, these results frame glassy matrices not merely as viable alternatives but as strategically advantageous hosts, capable of bridging fundamental photonic performance with scalable, device-level implementation in solar fuel technologies.

Table 3 summarizes representative photocatalytic and PEC water-splitting performances of Ln-based UC systems. The associated design strategies, structure–property relationships, and key findings from each entry are discussed in detail in Sections 2.3 and 2.4.

3. TTA-based upconversion in photocatalytic systems

3.1 Mechanism of triplet–triplet annihilation upconversion in photocatalytic systems

Triplet–triplet annihilation upconversion (TTA-UC) is a process in which two (or more) low-energy photons are converted into a higher-energy photon, enabling light's anti-Stokes shifting.[82] As illustrated schematically in Fig. 2, a sensitizer absorbs a sub-bandgap photon since most photocatalysts cannot absorb it themselves. Using the absorbed photon energy, an electron in a singlet ground state is promoted to a higher excited state, followed by an intersystem crossing (ISC) from the singlet excited state to the triplet state.[82] To transfer the long-lived triplet energy to an annihilator (emitter or acceptor), a triplet–triplet energy transfer (TET) is performed *via* Dexter exchange coupling.[82] The final step of triplet–triplet annihilation consists of the formation of one higher-energy excited singlet state and one ground state, when two annihilation molecules in their triplet state are combined.[82] The formed excited singlet of the annihilator then emits a delayed fluorescence at a shorter wavelength than the initially absorbed photon wavelength, and it is the upconverted photon, appearing as an anti-Stokes emission.[82] In photocatalytic systems that will be discussed below, the upconverted emission is developed to be in the absorption range of a semiconductor photocatalyst. Photocatalysts can absorb the upconverted, higher-energy (lower-frequency) photons and produce photogenerated charge

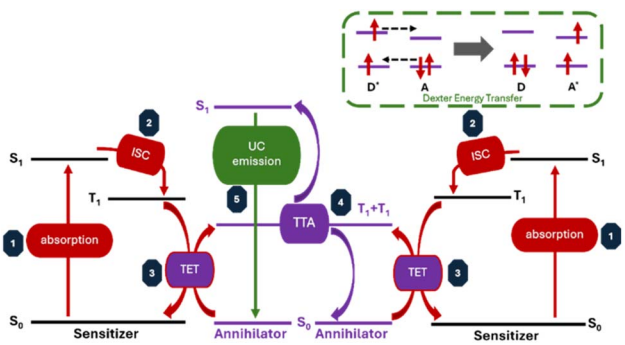

Fig. 2 Step-by-step TTA-UC mechanism illustration.

carriers to drive oxygen and hydrogen evolution reactions or pollutant degradation. However, to promote the transfer of upconverted energy into the photocatalytic reaction, the annihilator's emission spectrum has to match the band-gap absorption of the photocatalyst.[83] In addition, many UC systems incorporate the sensitizer/emitter pair in an oxygen-impermeable matrix or degassed medium to avoid quenching by oxygen, maintaining triplet lifetimes.[84] Overall, the TTA-based UC mechanism enables photocatalytic activity under a wider range of wavelengths by *in situ* generation of higher-energy photons from absorbed lower-energy ones, overcoming bandgap limitations of photocatalysts.

Considering lanthanide-doped UC materials, they exhibit very long excited-state lifetimes (microsecond to millisecond range) due to their f–f electronic transitions, consequently requiring high excitation intensities for the energy migration.[27] However, triplet excitons in organic TTA-UC systems have much shorter lifetimes (nanosecond to microsecond range) and require two triplets to encounter each other before radiative decay. Importantly, to allow bimolecular triplet–triplet annihilation to occur, TTA emitters must have triplet lifetimes long enough. Therefore, TTA-UC systems, operating under low light, have a limited probability of annihilation due to the shorter lifetimes.[27] These longer excited-state lifetimes of lanthanide upconverters and shorter triplet lifetimes of TTA systems lead to various excitation and energy transfer properties in photocatalytic water splitting.[27]

3.2 Performance metrics for TTA-based UC systems

Evaluation of the TTA-UC system's efficiency in photocatalysis is based on both UC luminescence and photocatalytic efficiency measurements. The main performance metric of upconversion is an upconversion quantum yield, Φ_{UC}, the ratio of the number of high-energy photons emitted by the UC system to that of low-energy photons absorbed.[82] To calculate the Φ_{UC} experimentally, eqn (3) is used:

$$\Phi_{UC} = \Phi_{std}\left(\frac{A_{std}}{A_{unk}}\right)\left(\frac{I_{unk}}{I_{std}}\right)\left(\frac{\eta_{unk}}{\eta_{std}}\right)^2 \quad (3)$$

where A, I, and η are the absorbance, integrated photoluminescence intensity, and refractive index of the solvents, correspondingly, while the subscripts std and unk are indicated as reference and sample compounds, respectively.

While Φ_{UC} quantifies the optical upconversion itself, most studies investigate the enhancement in the photocurrent density, apparent quantum yield (AQY), applied bias photon-to-current efficiency (ABPE), and solar-to-hydrogen efficiency (STH) to investigate upconversion's impact on photocatalysis. The photocurrent density enhancement is a measure of charge carrier generation, which is evaluated by the increase in photocurrent that TTA-UC systems deliver under sub-bandgap illumination, compared to a bare photocatalyst. However, to investigate the photocatalytic systems deeper, AQY, representing the percentage of light-to-product conversion, is an important metric to assess. The AQY values can be reported at a specific wavelength, or for the solar spectrum, and for hydrogen production systems, it is calculated by the following equation:

$$\mathrm{AQY} = \frac{2 \times \text{the number of evolved } H_2 \text{ molecules}}{\text{the number of incident photons(N)}} \quad (4)$$

where the number of incident photons is calculated from the average intensity of irradiation (E), wavelength (λ), Planck's constant (h), and the speed of light (c):

$$N = \frac{E\lambda}{hc} \quad (5)$$

These are the main parameters reported by the works related to solar water splitting and presented below. However, some of the reported results also evaluate ABPE, a measure of the efficiency of converting incident illumination to hydrogen under a certain applied bias, which is applicable only to the photoelectrochemical (PEC) water splitting characterization. For overall unbiased water splitting, the STH is also important since it measures the fraction of solar energy converted to chemical energy in the produced hydrogen. In photocatalytic pollutant degradation, the metrics, such as pseudo-first-order rate constants and percentage degradation over time, are mainly reported. Additionally, TTA-UC systems should have good cyclability, which is tested *via* testing over multiple cycles, to prove that the photocatalyst and sensitizer/emitter pair is not degrading during the test.

3.3 TTA-based UC systems for solar water-splitting

TTA-upconversion has been coupled with different photocatalysts for water splitting, aiming to utilize visible light to drive hydrogen (or oxygen) generation on UV-responsive semiconductors or to extend visible-light semiconductors further into the red/NIR. Table 4 summarizes reported systems since 2016.

CdS and its compounds ($Cd_xZn_{1-x}S$) based photocatalysts have a bandgap between 2.4 and 2.8 eV, which is equivalent to the absorption range of up to 520 nm. TTA-UC has been widely used to make these photocatalysts active under longer wavelengths (green or red-light region). In 2016, Ye *et al.*[84] paired Pd(II) tetraphenylporphyrin (PdTPP) sensitizer and 9,10-diphenylanthracence (DPA) emitter with $Cd_{0.7}Zn_{0.3}S$ photoanode and proved a concept of green-to-blue upconversion. The upconversion quantum yield, Φ_{UC}, achieved 36%, but the photocurrent density was presented just for the demonstration of the possibility of using it due to its low values. The second sensitizer/emitter pair, consisting of platinum-octaethylporphyrin (PtOEP) and DPA, was integrated into a decorated CdS photocathode, resulting in an enhanced photocurrent and 0.57% photon conversion efficiency under visible light irradiation.[85] Compared to bare CdS, green light upconversion to CdS-absorbable blue light showed a more substantial hydrogen production. To further enhance the effect of TTA-UC systems, Fang *et al.* embedded 3% Au nanoparticles with the same UC pair of PtOEP/DPA on g-C_3N_4-CdS photocatalyst to amplify the local excitation field.[87] The designed structure had a 2.2-fold enhancement in the upconversion intensity of green to blue

Table 4 TTA-based UC systems developed for solar water-splitting

Year	Photocatalytic system	TTA upconversion pair (sensitizer/emitter)	Excitation wavelength range	Enhancement in photocurrent density	Enhancement in H_2/O_2 production	Other performance metrics	Ref.
2016	$Cd_{0.7}Zn_{0.3}S$	PdTPP/DPA	532 nm	−(0.09 μA cm^{-2})	—	UC efficiency Φ_{UC} ~36%	Ye *et al.*[84]
2017	2 wt% rGO/CdS/SNC	PtOEP/DPA	526 nm	—	—	—	Chandrasekaran *et al.*[85]
			1-sun (Xe lamp, 100 mW cm^{-2})	−~0.123 mA cm^{-2} at 1.750 V *vs.* RHE	—	Photon conversion efficiency η ~0.57%	
2019	Mo-doped $BiVO_4$	Perylene/PdTPBP fluorophores in a PU matrix	600–650 nm	+17% (5.25 mA cm^{-2} at 1.23 V *vs.* RHE)	+16% (~100 μmol per cm^2 per h H_2 & ~45 μmol per cm^2 per h O_2)	ABPE 2.1% (+46% compared to bare Mo:$BiVO_4$ at 0.7 V_{RHE})	Choi *et al.*[86]
2019	g-C_3N_4-CdS	3% Au-PtOEP/DPA@SiO_2@0.5NC2	535 nm	—	−(0.551 mmol per g H_2 in 3 h)	AQY 1.493%	Fang *et al.*[87]
			>420 nm (visible light)		+168% (16.88 mmol per g H_2 in 3 h)	AQY 0.225% >90% stable H_2 production after 60 h	
2019	TiO_2	BA/PPO	445 nm	+800% (4.5 μA cm^{-2} at 0.4 V *vs.* Ag/AgCl)	−(~0.7 μmol per h H_2 at 0.6 V *vs.* Ag/AgCl)	—	Barawi *et al.*[88]
2019	$Cd_{0.5}Zn_{0.5}S$	PdTPTBP/BPEA	629 nm	—	−(~2.3 μL H_2 in 5 h)	AQY < 0.1%	Yu *et al.*[89]
2021	Mo:$BiVO_4$	PtOEP/DPA	535 nm	—	+28.9% (0.49 μmol h^{-1})	AQY < 0.01%	Kageshima *et al.*[90]
2023	$Cd_{0.5}Zn_{0.5}S$	PtOEP/PdTPTBP/PdTPNEt2P/perylene	>420 nm	—	+100% (8.44 mmol g^{-1} h^{-1})	UC quantum efficiency 14.12%	Liu *et al.*[91]
2024	Cu_2O	PbS/rubrene/BCP/Ag	950 nm	−(0.003 mA cm^{-2} at 0 V *vs.* RHE)	—	—	Magazov *et al.*[92]
			1-sun (Xe lamp, 100 mW cm^{-2})	+56% (0.5 mA cm^{-2} at 0 V *vs.* RHE)			
2024	Self-assembled: $PDI^{2-/}PDI^{2-}$ spin-hybrid all-organic semiconductor	*In situ* TTA	1-sun (Xe lamp, 100 mW cm^{-2})	—	−(55.11 μmol per g per h H_2 & 18.37 μmol per g per h O_2)	STH 0.0806% AQY 1.96% at 550 nm	Lin *et al.*[93]
2025	Rh/Cr_2O_3/CoOOH/Al:$SrTiO_3$	Ir(coumarin-6)$_2$(acac)/TIPS naphthalene	455 nm	—	+61.7% (0.00537 μmol H_2 in 10 min)	Φ_{UC} 6.1%	Madbak *et al.*[26]
			470 nm		+208.8% (0.00231 μmol H_2 in 10 min)		
2025	5% Mo-doped $BiVO_4$ photoanode	SiO_2-capsulated PtOEP/DPA	1-sun (Xe lamp, 100 mW cm^{-2})	+15% (2.3 mA cm^{-2} at 1.23 V *vs.* RHE)	+25% (16.89 mmol per g per h H_2)	+18% ABPE 99% photodegradation efficiency of 10 mg per L enrofloxacin	Venkatesan *et al.*[94]

emission compared with the TTA-UC system without Au due to increased excitation-light absorption of 535 nm by the plasma resonance effect of Au. Achieving 16.88 mmol per g H_2 yield in 3 h, this work proved that the plasmonic effect in tandem with TTA-UC can significantly enhance the hydrogen generation under the red-light spectrum of CdS-based photocatalysts. However, efficient incorporation of PdTPTBP and 9,10-bis(phenylethynyl)anthracene (BPEA) pair together with $Cd_{0.5}Zn_{0.5}S$ was challenging due to triplet quenching by oxygen or imperfect spectral overlap, as evidenced by sub-0.1% AQY.[89] More recently, Liu *et al.*[91] demonstrated a multi-sensitizer approach on $Cd_{0.5}Zn_{0.5}S$, mixing PtOEP with two palladium porphyrins (PdTPTBP and $PdTPNEt_2P$) to absorb a broader range of visible light, with perylene as the emitter. The mixed sensitizers had a broader absorption, allowing >420 nm light more effective utilization. This gives attention to the usage of complementary sensitizers to harvest the full visible spectrum for CdS-based photocatalysts. Overall, CdS-based TTA-UC system shows promising enhancements in hydrogen generation, but the performance variation remains huge.

$BiVO_4$ is a widely studied photoanode for water oxidation with a bandgap of 2.4 eV. TTA-UC has been investigated to improve the activity of this photoanode beyond 520 nm. An enhanced photocurrent density at 1.23 V *vs.* RHE (+17%), and almost doubled ABPE values indicated a successful integration of PdTPBP/perylene upconverter behind a Mo-doped $BiVO_4$ electrode.[86] In 2021, Kageshima *et al.*[90] reported 29% higher O_2 yield under 535 nm light, adding a UC system comprising a PtOEP/DPA, but the AQY remained <0.01% because of weak emission and the demanding four-hole process. This year, 5% Mo-doped $BiVO_4$ was incorporated with SiO_2-capsulated PtOEP/DPA and used for both hydrogen production and enrofloxacin (ENR) photodegradation, highlighting multifunctionality.[94] Fluoroquinolones such as ENR are attacked primarily at the quinolone core and piperazine side chain. Hydroxyl ($^{\bullet}OH$) and superoxide ($O_2^{\bullet-}$) radicals cleave the piperazine ring and oxidize the fluoroquinolone ring, followed by a hydroxylation of aromatic carbons, dealkylation, and defluorination, resulting in smaller, less-toxic molecules.[95] The possible mechanism of ENR removal and simultaneous hydrogen production by Mo-doped $BiVO_4$ TTA-UC system proposed by the authors is shown in Fig. 3. These studies show that TTA-UC offers promising gains for $BiVO_4$ at longer wavelengths, but to progress further, improvements in light-trapping and Φ_{UC} in the red-to-blue range are required.

Wide-bandgap photocatalysts such as TiO_2 and $SrTiO_3$ cannot utilize visible light, thus, TTA-UC is a promising strategy to use with them. For example, Barawi *et al.*[88] coupled a TiO_2 photoelectrode with a 2,3-butanedione (biacetyl, BA)/2,5-diphenyloxazole (PPO) system, where BA absorbed visible light (430–450 nm), while PPO emitted the UV at 370 nm. After integration of the TTA-UC system, TiO_2 delivered a nine-fold photocurrent (4.5 *vs.* 0.5 μA cm^{-2} at 0.4 V *vs.* Ag/AgCl) under 445 nm excitation, proving that blue photons can be upconverted to match TiO_2's bandgap. Another ground-breaking UC approach was used on Al:$SrTiO_3$:Rh by integration of Ir(coumarin-6)$_2$(acac)/TIPS naphthalene pair to drive overall water splitting.[26] This allowed for an increase in the H_2 evolution under both 455 and 470 nm by 61.7% and 208%, respectively, whereas these wavelengths are unusable by bare $SrTiO_3$. However, the H_2 yields remain very low (nanomole scale), showing a possible research direction that has early proof-of-concept.

Other works investigating less conventional photocatalysts highlight the potential of incorporating NIR upconversion in solar water-splitting. For instance, Magazov *et al.*[92] enabled NIR-to-visible upconversion by coupling a Cu_2O photocathode with PbS sensitizer and rubrene/bathocuproine (BCP) annihilator pair. This approach allowed for harvesting infrared light,

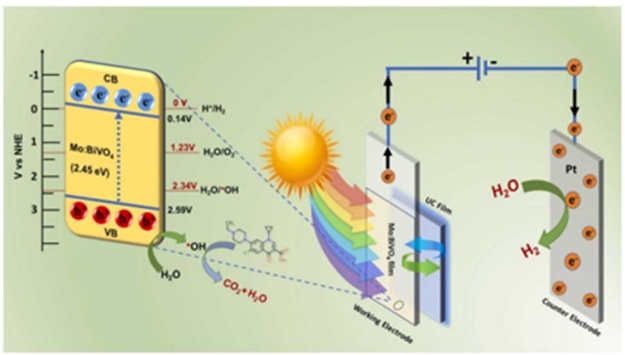

Fig. 3 The possible mechanism for the simultaneous photodegradation of ENR and H_2 generation by 5% Mo-doped $BiVO_4$ photoanode coupled with TTA-UC system under visible light irradiation. Reproduced from Venkatesan *et al.*,[96] copyright 2025 Elsevier B.V.

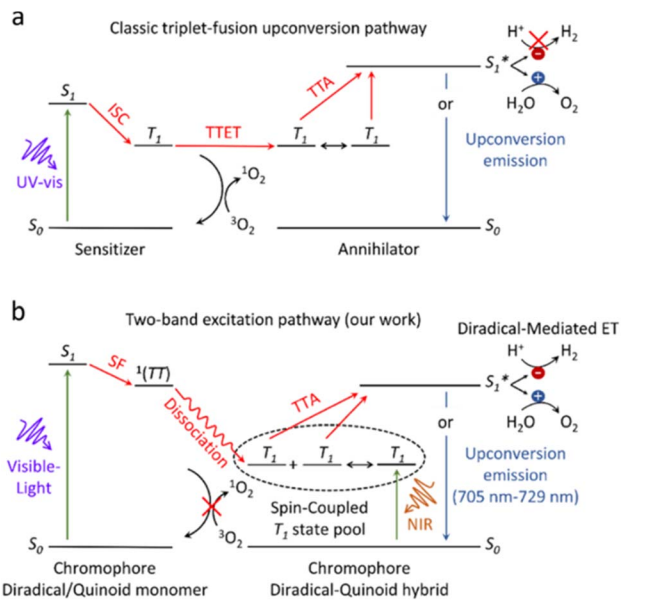

Fig. 4 (a) Organic sensitizer–annihilator system following the classic triplet-fusion upconversion mechanism through ISC, and (b) the two-band excitation upconversion mechanism in a spin-hybrid:PDI^{2-}/PDI^{2-} all-organic photocatalyst utilizing the full vis-to-NIR solar spectrum proposed by authors. Reproduced from Lin *et al.*,[93] copyright 2024 Springer Nature.

resulting in a small photocurrent under NIR and a 56% enhancement under full-spectrum illumination. Another promising work is related to assembling an all-organic perylene diimide semiconductor, which acts both as a photocatalyst and UC system.[93] The self-assembled system achieved overall water-splitting with 0.08% STH and 1.96% AQY under 550 nm illumination. Despite low efficiency and stability achieved, this work showed a breakthrough in combining light harvesting and catalysis in a single component. Additionally, compared to the classic triplet-fusion upconversion pathway used in most of the works, this all-organic semiconductor follows the two-band excitation upconversion pathway presented in Fig. 4.

Overall, the TTA-based UC system made a significant contribution to solar water-splitting by overcoming bandgap limitations. PEC cells and thin-film devices are promising since it is more practical to integrate the UC pair with them rather than in suspension systems. Currently, researchers are also working on developing multifunctional reactors aiming at H_2 production with pollutant degradation. In the future, the development of materials enabling larger anti-Stokes shifts and higher UC quantum yields will be important for integrating TTA-UC systems into large-scale, sustainable solar water-splitting technologies.

However, the major challenge for practical TTA-UC photocatalysts is still their stability under operation, since dye-sensitizer systems can photobleach or oxidize quickly. To solve the stability problem, recent studies have demonstrated enhancement in the durability of TTA-UC *via* its encapsulation in robust matrices. For example, Bharmoria *et al.*[97] incorporated a Pt(II) photosensitizer and organic annihilator into a biopolymer-surfactant hydrogel, protecting the TTA-UC system from oxygen quenching. This work showed how the dense hydrogen-bond network of the hydrogel prevented O_2 diffusion into the chromophore domains, resulting in stable upconversion efficiency in air. This is the general strategy to use functionalized organic gels and polymers embedding TTA chromophores and blocking oxygen access.[27] In addition to photostability improvements, protective matrices facilitate multiple reuse cycles without significant loss of activity.

3.4 TTA-based UC systems for photodegradation of organic pollutants

TTA upconversion has also been applied to photocatalytic degradation of pollutants, enabling the use of visible light to drive oxidative degradation on UV-activated photocatalysts. Table 5 summarizes reported systems targeting various organic pollutants.

Tetracycline (TC) is a challenging pollutant for photocatalytic degradation since it is highly resistant to direct photolysis under visible light. Similar to the ENR oxidation, the studies of oxidation processes indicate that reactive oxygen species (ROS) attack TC at specific molecular sites. The abstraction of hydrogen atoms from the aromatic rings of TC by $^{\bullet}OH$ and their addition to unsaturated bonds initiates ring-opening reactions. Consequently, based on the presented computational work, these $^{\bullet}OH$-mediated pathways break the

Table 5 TTA-based UC systems developed for the photodegradation of organic pollutants

Year	Photocatalytic system	TTA upconversion pair (sensitizer/emitter)	Excitation wavelength range	Target pollutant	Photodegradation performance	Ref.
2016	ND-loaded WO_3	20 wt% AgNP–SiO_2/ PtOEP/DPA	532 nm	Acetaldehyde	~100% degradation of 20 ppmv acetaldehyde in 3 h	Kim *et al.*[98]
2017	Pt@CdS	PtOEP/DPA@SiO_2	520 nm	Tetracycline	Pseudo-first-order degradation rate constant k_{pfo} 0.0061 44% degradation in 100 min Φ_{UC} 0.0777%	Fang *et al.*[99]
			Visible-light region		k_{pfo} 0.01118 66% degradation in 100 min Φ_{UC} 0.0341%	
2020	G/CdS	0.3 AuNPs-PtOEP/DPA in PDMS film	Visible-light region	Tetracycline	k_{pfo} 0.294 h^{-1} 90% degradation in 3 h Stability over 5 cycles	Fang *et al.*[100]
2020	g-C_3N_4@CdS	AuNPs-PtOEP/DPA in PDMS	Visible light	Tetracycline	k_{pfo} 0.446 h^{-1} Stable 90% degradation after 5 cycles	Fang *et al.*[28]
2023	CdS	Au-PtOEP/DPA on a PVDF	535 nm	Isopropanol	Quantum yield 11.05% Stable 90% degradation after 5 cycles	Fang *et al.*[101]
2024	Pt-WO_3/GO-Si reflector	PdOEP/DPA	550 nm	4-Chlorophenol	K_d 86.52 × 104 min^{-1} Stable >55% degradation after 5 cycles	Cho *et al.*[102]
				Bisphenol A	K_d 144.97 × 104 min^{-1} Stable >70% degradation after 5 cycles	
				Methylene blue	K_d 307.48 × 104 min^{-1} Stable > 90% degradation after 5 cycles	

TC structure into small fragments, leading to CO_2, H_2O, and low-molecular-weight carboxylic acids.[103] For example, Fang *et al.*[99] used a widely studied CdS photocatalyst with PtOEP/DPA upconversion system, enabling 44% removal of TC in 100 min under green light irradiation compared to negligible activity of bare CdS. Nevertheless, the UC quantum yield was low (<0.1%), promoting subsequent studies, which incorporated plasmonic Au nanoparticles, graphene, and photonic crystal films with enhanced upconversion efficiency and photocatalytic activity. For example, Au-graphene/CdS composites in a PDMS matrix showed 90% TC removal in 3 h, whereas photonic-crystal assisted design further increased the rate to $k = 0.446\ h^{-1}$ with stable photodegradation performance over five cycles.[28,100] By 2023, optimized films of CdS with the TTA-UC system achieved Φ_{UC} 11%, enabling 90% photodegradation of isopropanol under 535 nm light.[101]

Other presented works also focused on volatile organic compounds, such as acetaldehyde. Kim *et al.*[98] presented a gas phase pollutant removal using WO_3 photocatalyst modified with nanodiamonds and combined with Ag@SiO_2-PtOEP/DPA TTA-UC system. Bare WO_3 is normally inactive under green light, but coupled with the UC system, it reached 100% photodegradation of 20 ppmv acetaldehyde in 3 h under 532 nm irradiation. However, to reach this efficiency, the system required Ag@SiO_2 engineered structures and high PtOEP loading. The same photocatalyst was coupled with PdOEP/DPA TTA-UC system, converting 550 nm light into 430 nm.[102] Pt-WO_3 photocatalyst with TTA-UC achieved >55%, >70%, and >90% removal for 4-chlorophenol, bisphenol A, and methylene blue, respectively, over five cycles. In the developed system, the graphene oxide layer-covered Si photonic crystal stop-band enhanced light trapping at the UC emission wavelength, whereas Pt cocatalyst improved charge separation, as shown in Fig. 5. Overall, the presented results of tetracycline, VOCs, and other pollutants photodegradation present a promising practical tool for environmental remediation using TTA-UC systems since these systems are driving oxidation processes by harvesting visible light.

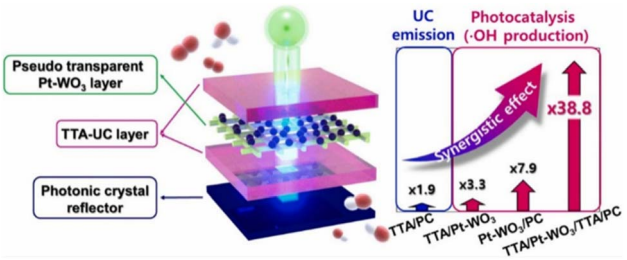

Fig. 5 Schematic illustration of the TTA/Pt-WO_3/TTA/Photonic crystal multi-layered sub-bandgap photocatalytic reactor. UC emission enhancement is analyzed compared the full TTA-UC system, while the $^{\bullet}OH$ generation efficiency for photooxidation of pollutants is compared to that of the Pt-WO_3 layer in each combination. Reproduced from Cho *et al.*,[102] copyright 2024 Elsevier B.V.

4. Comparison of Ln-UC and TTA-UC systems

In PEC water splitting, Ln-UC and TTA-UC provide complementary routes to harvest sub-band-gap photons, but each

Table 6 Comparison of Ln-UC and TTA-UC for PEC water splitting. Abbreviations: ESA = excited-state absorption; ETU = energy-transfer upconversion; TET = triplet energy transfer; ISC = intersystem crossing

	Ln-UC (lanthanide-doped phosphors)	TTA-UC (organic dye systems)
Mechanism	4f–4f multiphoton process in doped hosts; ESA/ETU between real metastable 4f levels	Sensitizer absorbs → ISC to T_1 → dexter TET to annihilator T_1 → bimolecular TTA → emissive S_1
Anti-Stokes shift	Large energy upshifts (*e.g.*, Tm^{3+} → UV/blue)	Smaller energy upshifts
Excitation	NIR: 980 nm (Yb^{3+}); 808 nm (Nd^{3+})	Vis-NIR (depends on sensitizer/annihilator pair)
Spectral tunability	Limited (set by dopant/host; narrow lines)	Highly tunable emission color *via* dye chemistry
Excitation bandwidth	Narrow absorption lines; small absorption cross-section	Broad absorption; large cross-section; easy LED matching
Rate-limiting process	Population of intermediate 4f levels; cross-relaxation/ETU kinetics	Triplet diffusion and bimolecular annihilation; TET efficiency
Typical host/form	Fluorides ($NaYF_4$), oxides (Y_2O_3), garnets (YAG/YAP); nanoparticles, powders, ceramics	Organic dyes in solution, polymer matrices, solid films; MOF/micelle encapsulation
Oxygen tolerance	Not affected by O_2; operates in air/water	Triplets are strongly O_2-quenched
Photostability	Thermally/chemically robust; resists photobleach	Variable; dyes can photobleach without protection
Chemical robustness	Highly chemically stable inorganic solids	O_2-sensitive; suffers quenching and photodegradation in the absence of protection
Production maturity	Well-established syntheses; scalable and cost-manageable	Manufacturing/standardization is still emerging; encapsulation adds complexity
Key limitations	Modest conversion at low irradiance; poor spectral tunability; 980 nm can cause thermal heating of water (prefer 808 nm); photonic/plasmonic coupling can be necessary	Sensitive to oxygen (encapsulation needed); dye photodegradation occurs; slurry implementation impractical; metrics controlled by film morphology
Key advantages	Robust/O_2-stable; UV emission possible; works in slurries; mature synthesis	Operates at low irradiance (LED/1-sun); color-tunable; integrates well with thin films and PEC cells

mechanism defines its own operating window and integration limits. Table 6 summarizes those differences and shows when each platform is the better fit. Ln-based UC is durable and photostable for harvesting sub-bandgap photons, but without photonic assistance, it can be intensity-limited under one sun. In contrast, TTA-UC delivers tunable spectra and low-irradiance operation but requires reliable oxygen exclusion. These contrasts frame the practical choices for device design.[104,105]

Reflecting these differences, AM1.5G analyses show Ln-UC generally needs ≥1–2 orders-of-magnitude photophysical improvements or significant photon recycling/concentration, whereas TTA-UC can approach a near-linear regime at one sun using high-extinction NIR sensitizers and long-lived, diffusive triplets, enabling measurable PEC benefits.[106,107]

When chemical environment and durability are considered, the preference reverses. TTA-UC uses molecular triplets that are quenched by O_2, so it needs tight barriers, microencapsulation, or separation from the OER region, with additional limits from photobleaching and radical chemistry. Ln-UC employs protected 4f centers in inorganic lattices, giving high photostability in aqueous/oxidative electrolytes; quenching mainly arises from high-energy vibrations and defects and can be mitigated with fluoride hosts and robust shells. For long-term operation, Ln-UC is preferable.[108,109]

In summary, applications should be tailored to mechanisms. TTA-UC is suitable for near-solar irradiance when oxygen is well controlled and blue or near-UV emission. Its recent PEC demonstrations and tunability make it a promising route to incremental device gains. Ln-UC is advantageous where chemical robustness and long operation in solutions are essential, or where photonic concentration or recycling is available and non-980-nm sensitization is used to avoid heating in water. In either strategy, the upconverter and optical stack should be designed together, with results presented under uniform, solar-relevant tests to verify meaningful device-level gains.

5. Conclusions

Both lanthanide-based and TTA-based upconversion approaches offer promising pathways to overcome the solar spectrum losses that limit conventional photocatalysis. Lanthanide-doped upconversion materials can extend a photocatalyst's activity into the near-infrared domain, tapping a vast reservoir of sub-bandgap photons that would otherwise go unused. Studies have shown that such Ln upconverters (Yb^{3+}/Er^{3+}-doped phosphors) are capable of driving hydrogen generation from NIR excitation, underscoring their fundamental viability for solar fuel applications. Moreover, their inorganic nature lends them favorable stability under photocatalytic conditions. However, the efficiency of lanthanide upconversion under ambient sunlight remains a primary concern. Owing to the small absorption cross-sections and multiphoton excitation requirements of f-element ions, UC emission intensities are very low at 1-sun illumination in the absence of light concentration. As a result, the overall impact of Ln-based upconversion on solar water-splitting efficiency has so far been modest. By contrast, TTA-based upconversion systems have demonstrated the ability to efficiently convert lower-energy visible photons to higher-energy emission even at solar photon flux levels. These molecular upconverters have already achieved significant performance gains when coupled to photocatalysts – for example, improving photocurrents by over 50% in a hybrid photoelectrode device – and uniquely, a suitably engineered TTA system has even enabled overall water splitting using only low-energy visible light inputs. Such results highlight the impact of TTA upconversion in accessing a broader swath of the solar spectrum. On the other hand, the practical deployment of TTA upconversion will require surmounting challenges related to chemical stability and continuous operation. The short operational lifetimes observed for current TTA-UC materials (on the order of minutes before performance degrades) serve as a reminder that new, more robust emitter/sensitizer combinations or solid-state encapsulation strategies are needed.

Comparing the two upconversion paradigms reveals a complementary set of strengths and weaknesses. Ln-based upconverters excel in spectral reach – they can harvest photons in the deep red and IR range (λ > 800 nm) that are largely inaccessible to TTA systems – and they integrate well with solid inorganic catalysts as particulate additives or transparent layers. However, their low luminescence efficiencies under unconcentrated light and fixed excitation bands (dictated by 4f energy levels) limit their contribution unless enhanced by external means. TTA-based upconverters, in contrast, offer high quantum efficiency under low irradiance, and their absorption/emission profiles are tunable through molecular design, allowing customization for different photocatalyst bandgaps. The trade-off is that TTA systems involve more complex chemistry (often requiring deoxygenation and specialized solvents or polymer hosts) and can suffer from limited durability. In many ways, the two approaches can be viewed as complementary: for instance, a lanthanide phosphor could capture and upconvert deep IR photons, while a TTA system handles lower-energy visible photons – together covering a wider solar range than either alone. Looking ahead, future research should aim to combine the strengths of both strategies while mitigating their limitations. For Ln-based materials, this includes pursuing luminescence enhancement techniques (such as incorporating plasmonic nanostructures or optimizing core–shell architectures) to boost their emission under solar conditions. For TTA systems, developing new sensitizer–emitter pairs that are active in the red/NIR, as well as robust matrices (*e.g.*, metal–organic frameworks or solid films) that protect against oxygen and photodegradation, will be crucial for long-term operation. Equally important is the engineering integration of upconversion materials into water-splitting devices – for example, constructing tandem absorber configurations or placing upconverters in optical contact with photoelectrodes to ensure efficient transfer of the upconverted photons to the catalyst. With continued advances, upconversion-assisted designs could progressively raise the solar-to-hydrogen (STH) efficiency of photocatalytic systems toward the 10% benchmark viewed as necessary for commercial viability. In summary, upconversion materials represent a new frontier in solar water splitting, offering a powerful means to unlock the unused portions of the

solar spectrum and drive green hydrogen production with greater efficiency. By leveraging and improving both Ln-based and TTA-based upconversion in complementary ways, the photocatalysis community can move closer to the goal of economically sustainable solar fuel generation.

Author contributions

Y. M. – conceptualization, drafted the initial manuscript, review, and editing the manuscript. A. A., N. Z., Z. T. – data curation, writing, review, and editing the manuscript. G. Z., N. N. – supervision, writing, review, and editing the manuscript. All authors have given approval to the final version of the manuscript.

Conflicts of interest

The authors declare that there is no conflicts of interest.

Data availability

No primary research results, software, or code have been included, and no new data were generated or analyzed as part of this review.

Acknowledgements

This work was supported by the Science Committee of the Ministry of Science and Higher Education of the Republic of Kazakhstan (Grant No. AP27511221 and Grant No. BR21882439). The authors acknowledge the financial support from the INESS-2025 Organizing Committee and the NU Impact Foundation of Nazarbayev University, which covered the article processing charge for this publication.

References

1 C. Jiang, S. J. A. Moniz, A. Wang, T. Zhang and J. Tang, Photoelectrochemical devices for solar water splitting-materials and challenges, *Chem. Soc. Rev.*, 2017, **46**, 4645–4660.
2 K. T. Fountaine, H. J. Lewerenz and H. A. Atwater, Efficiency limits for photoelectrochemical water-splitting, *Nat. Commun.*, 2016, **7**, 13706.
3 L. Liao, Q. Zhang, Z. Su, Z. Zhao, Y. Wang, Y. Li, X. Lu, D. Wei, G. Feng, Q. Yu, X. Cai, J. Zhao, Z. Ren, H. Fang, F. Robles-Hernandez, S. Baldelli and J. Bao, Efficient solar water-splitting using a nanocrystalline CoO photocatalyst, *Nat. Nanotechnol.*, 2014, **9**, 69–73.
4 Y. Magazov, A. Aliyev, K. Moldabekov, A. Kurbanova, A. Rakymbekova, M. Amze, N. Ibrayev and V. Kudryashov, Photoelectrochemical Water Splitting Using Cuprous Oxide (Cu2O)-Based Photocathode – A Review, *ES Energy & Environment*, 2024, **26**, 1347.
5 Y. Magazov, V. Kudryashov, D. D. Asmatulu and N. Nuraje, in *Nanotechnology Safety*, ed. R. Asmatulu, W. S. Khan and E. Asmatulu, Elsevier, 2nd edn, 2025, pp. 321–333.
6 R. Memmino, Solar Energy Conversion By Photoelectrochemical Processes, *Electrochim. Acta*, 1980, **25**, 77–88.
7 A. J. Bard and M. A. Fox, Artificial Photosynthesis: Solar Splitting of Water to Hydrogen and Oxygen, *Acc. Chem. Res.*, 1995, **28**, 141–145.
8 M. Grätzel, Photoelectrochemical cells, *Nature*, 2001, **414**, 338–344.
9 B. K. Meyer, A. Polity, D. Reppin, M. Becker, P. Hering, P. J. Klar, T. Sander, C. Reindl, J. Benz, M. Eickhoff, C. Heiliger, M. Heinemann, J. Bläsing, A. Krost, S. Shokovets, C. Müller and C. Ronning, Binary copper oxide semiconductors: From materials towards devices, *Phys. Status Solidi B*, 2012, **249**, 1487–1509.
10 W. Niu, T. Moehl, W. Cui, R. Wick-Joliat, L. Zhu and S. D. Tilley, Extended Light Harvesting with Dual Cu2O-Based Photocathodes for High Efficiency Water Splitting, *Adv. Energy Mater.*, 2018, **8**, 1702323.
11 S. Siol, J. C. Hellmann, S. D. Tilley, M. Graetzel, J. Morasch, J. Deuermeier, W. Jaegermann and A. Klein, Band Alignment Engineering at Cu2O/ZnO Heterointerfaces, *ACS Appl. Mater. Interfaces*, 2016, **8**, 21824–21831.
12 K. Afroz, M. Moniruddin, N. Bakranov, S. Kudaibergenov and N. Nuraje, A heterojunction strategy to improve the visible light sensitive water splitting performance of photocatalytic materials, *J. Mater. Chem. A*, 2018, **6**, 21696–21718.
13 A. Paracchino, N. Mathews, T. Hisatomi, M. Stefik, S. D. Tilley and M. Grätzel, Ultrathin films on copper(i) oxide water splitting photocathodes: A study on performance and stability, *Energy Environ. Sci.*, 2012, **5**, 8673–8681.
14 M. Moniruddin, E. Oppong, D. Stewart, C. McCleese, A. Roy, J. Warzywoda and N. Nuraje, Designing CdS-Based Ternary Heterostructures Consisting of Co-Metal and CoOx Cocatalysts for Photocatalytic H2 Evolution under Visible Light, *Inorg. Chem.*, 2019, **58**, 12325–12333.
15 S. D. Tilley, M. Schreier, J. Azevedo, M. Stefik and M. Graetzel, Ruthenium oxide hydrogen evolution catalysis on composite cuprous oxide Water-splitting photocathodes, *Adv. Funct. Mater.*, 2014, **24**, 303–311.
16 C. G. Morales-Guio, S. D. Tilley, H. Vrubel, M. Grätzel and X. Hu, Hydrogen evolution from a copper(I) oxide photocathode coated with an amorphous molybdenum sulphide catalyst, *Nat. Commun.*, 2014, **5**, 3059.
17 M. N. I. Salehmin, L. Jeffery Minggu, W. F. Mark-Lee, M. A. Mohamed, K. Arifin, M. H. H. Jumali and M. B. Kassim, Highly photoactive Cu2O nanowire film prepared with modified scalable synthesis method for enhanced photoelectrochemical performance, *Sol. Energy Mater. Sol. Cells*, 2018, **182**, 237–245.
18 J. Luo, L. Steier, M. K. Son, M. Schreier, M. T. Mayer and M. Grätzel, Cu2O Nanowire Photocathodes for Efficient and Durable Solar Water Splitting, *Nano Lett.*, 2016, **16**, 1848–1857.
19 L. Pan, J. H. Kim, M. T. Mayer, M. K. Son, A. Ummadisingu, J. S. Lee, A. Hagfeldt, J. Luo and M. Grätzel, Boosting the

performance of Cu2O photocathodes for unassisted solar water splitting devices, *Nat. Catal.*, 2018, **1**, 412–420.

20 J. Bai, Y. Li, R. Wang, K. Huang, Q. Zeng, J. Li and B. Zhou, A novel 3D ZnO/Cu2O nanowire photocathode material with highly efficient photoelectrocatalytic performance, *J. Mater. Chem. A*, 2015, **3**, 22996–23002.

21 I. R. Hamdani and A. N. Bhaskarwar, Cu2O nanowires based p–n homojunction photocathode for improved current density and hydrogen generation through solar-water splitting, *Int. J. Hydrogen Energy*, 2021, **46**, 28064–28077.

22 F. (Feng) Tao, W. F. Schneider and P. V. Kamat, *Heterogeneous Catalysis at Nanoscale for Energy Applications*, Wiley, 2015.

23 F. Auzel, Upconversion and Anti-Stokes Processes with f and d Ions in Solids, *Chem. Rev.*, 2004, **104**, 139–174.

24 Q. Zhang, F. Yang, Z. Xu, M. Chaker and D. Ma, Are lanthanide-doped upconversion materials good candidates for photocatalysis?, *Nanoscale Horiz.*, 2019, **4**, 579–591.

25 F. Wang and X. Liu, Upconversion Multicolor Fine-Tuning: Visible to Near-Infrared Emission from Lanthanide-Doped NaYF4 Nanoparticles, *J. Am. Chem. Soc.*, 2008, **130**, 5642–5643.

26 E. Madbak, D. J. Osborn, T. Small, T. Ishwara, T. W. Schmidt, K. Domen and G. F. Metha, Utilising triplet-triplet annihilation upconversion for overall photocatalytic water splitting, *Chem. Commun.*, 2024, **61**, 157–160.

27 M. Bucchieri, F. S. Freyria and B. Bonelli, Triplet-triplet annihilation upconversion sensitized with nanocrystals for a new generation of photocatalytic systems, *J. Mater. Chem. A*, 2025, **13**, 18115–18145.

28 J. Fang, Y. Chen, C. Zhu, X. Li, W. Wang, C. Lu, Y. Ni, L. Fang and Z. Xu, Enhanced triplet-triplet annihilation upconversion by photonic crystals and Au plasma resonance for efficient photocatalysis, *Catal. Sci. Technol.*, 2020, **10**, 8325–8331.

29 B. Yao, H. Sun, Y. He, S. Wang and X. Liu, Recent Advances in the Photoreactions Triggered by Porphyrin-Based Triplet–Triplet Annihilation Upconversion Systems: Molecular Innovations and Nanoarchitectonics, *Int. J. Mol. Sci.*, 2022, **23**, DOI: 10.3390/ijms23148041.

30 A. Mavridi-Printezi, A. Menichetti, M. Guernelli and M. Montalti, Extending photocatalysis to the visible and NIR: The molecular strategy, *Nanoscale*, 2021, **13**, 9147–9159.

31 B. Li, Y. Hu, Z. Shen, Z. Ji, L. Yao, S. Zhang, Y. Zou, D. Tang, Y. Qing, S. Wang, G. Zhao and X. Wang, Photocatalysis Driven by Near-Infrared Light: Materials Design and Engineering for Environmentally Friendly Photoreactions, *ACS ES&T Eng.*, 2021, **1**, 947–964.

32 L. Jiang, J. Yang, S. Zhou, H. Yu, J. Liang, W. Chu, H. Li, H. Wang, Z. Wu and X. Yuan, Strategies to extend near-infrared light harvest of polymer carbon nitride photocatalysts, *Coord. Chem. Rev.*, 2021, **439**, 213947.

33 J. Zhao, K. Xu, W. Yang, Z. Wang and F. Zhong, The triplet excited state of Bodipy: Formation, modulation and application, *Chem. Soc. Rev.*, 2015, **44**, 8904–8939.

34 X. Li and M. L. Tang, Triplet transport in thin films: fundamentals and applications, *Chem. Commun.*, 2017, **53**, 4429–4440.

35 K. Zhang, M. Zhou, C. Yu, X. Li, K. Yang, S. Yang, W. Dai, W. Huang, Q. Fan and L. Zhu, High value-added fluorescence upconversion agents-assisted nano-semiconductors for efficient wide spectral response photocatalysis: Exerting energy transfer effect and applications, *J. Rare Earths*, 2021, **39**, 243–260.

36 L. Schumacher and R. Marschall, Recent Advances in Semiconductor Heterojunctions and Z-Schemes for Photocatalytic Hydrogen Generation, *Top. Curr. Chem.*, 2022, **380**, 53.

37 L. Jiang, S. Zhou, J. Yang, H. Wang, H. Yu, H. Chen, Y. Zhao, X. Yuan, W. Chu and H. Li, Near-Infrared Light Responsive TiO_2 for Efficient Solar Energy Utilization, *Adv. Funct. Mater.*, 2022, **32**, 2108977.

38 J. Prakash, Samriti, A. Kumar, H. Dai, B. C. Janegitz, V. Krishnan, H. C. Swart and S. Sun, Novel rare earth metal–doped one-dimensional TiO_2 nanostructures: Fundamentals and multifunctional applications, *Mater. Today Sustain.*, 2021, **13**, 100066.

39 O. Iqbal, H. Ali, N. Li, A. I. Al-Sulami, K. F Alshammari, H. S. M. Abd-Rabboh, Y. Al-Hadeethi, I. U. Din, A. I. Alharthi, R. Altamimi, A. Hayat and M. Zahid Ansari, A review on the synthesis, properties, and characterizations of graphitic carbon nitride (g-C_3N_4) for energy conversion and storage applications, *Mater. Today Phys.*, 2023, **34**, 101080.

40 W. Fan, H. Bai and W. Shi, Semiconductors with NIR driven upconversion performance for photocatalysis and photoelectrochemical water splitting, *CrystEngComm*, 2014, **16**, 3059–3067.

41 A. Nadort, J. Zhao and E. M. Goldys, Lanthanide upconversion luminescence at the nanoscale: fundamentals and optical properties, *Nanoscale*, 2016, **8**, 13099–13130.

42 J. Shi, J. Ye, L. Ma, S. Ouyang, D. Jing and L. Guo, Site-selected doping of upconversion luminescent Er 3+ into SrTiO 3 for visible-light-driven photocatalytic H 2 or O 2 evolution, *Chem.—Eur. J.*, 2012, **18**, 7543–7551.

43 S. Wang, R. Deng, H. Guo, S. Song, F. Cao, X. Li, S. Su and H. Zhang, Lanthanide doped Y6O5F8/YF3 microcrystals: Phase-tunable synthesis and bright white upconversion photoluminescence properties, *Dalton Trans.*, 2010, **39**, 9153–9158.

44 S. Wang, S. Su, S. Song, R. Deng and H. Zhang, Raisin-like rare earth doped gadolinium fluoride nanocrystals: Microwave synthesis and magnetic and upconversion luminescent properties, *CrystEngComm*, 2012, **14**, 4266–4269.

45 L. Yin, Y. Li, J. Wang, Y. Zhai, J. Wang, Y. Kong, B. Wang and X. Zhang, Preparation of Er3+:Y3Al5O 12/TiO2-ZnO composite and application of solar energy in

photocatalytic degradation of organic dyes, *Environ. Prog. Sustainable Energy*, 2013, **32**, 697–704.

46 W. Wang, W. Huang, Y. Ni, C. Lu, L. Tan and Z. Xu, Graphene supported βnaYF 4 :Yb 3+ ,Tm 3+ and N doped P25 nanocomposite as an advanced NIR and sunlight driven upconversion photocatalyst, *Appl. Surf. Sci.*, 2013, **282**, 832–837.

47 X. Wu, S. Yin, Q. Dong, B. Liu, Y. Wang, T. Sekino, S. W. Lee and T. Sato, UV, visible and near-infrared lights induced NOx destruction activity of (Yb,Er)-NaYF4/C-TiO2 composite, *Sci. Rep.*, 2013, **3**, 2918.

48 C. Li, F. Wang, J. Zhu and J. C. Yu, NaYF4:Yb,Tm/CdS composite as a novel near-infrared-driven photocatalyst, *Appl. Catal., B*, 2010, **100**, 433–439.

49 Z. Li, C. Li, Y. Mei, L. Wang, G. Du and Y. Xiong, Synthesis of rhombic hierarchical YF3 nanocrystals and their use as upconversion photocatalysts after TiO2 coating, *Nanoscale*, 2013, **5**, 3030–3036.

50 S. Huang, L. Gu, C. Miao, Z. Lou, N. Zhu, H. Yuan and A. Shan, Near-infrared photocatalyst of Er3+/Yb3+ codoped (CaF2@TiO2) nanoparticles with active-core/active-shell structure, *J. Mater. Chem. A*, 2013, **1**, 7874–7879.

51 R. B. Cevallos-Toledo, D. Bellezza, J. Ferrera-González, A. Giussani, E. Ortí, M. González-Béjar and J. Pérez-Prieto, Cooperative Sensitization Upconversion in Ytterbium(III)-Based Eosin Lake Pigments, *ChemPhotoChem*, 2023, **7**, e202300156.

52 S. Aggarwal, Recent advances in fundamental research on photon avalanches on the nanometre scale, *Nanoscale*, 2025, **17**, 6329–6361.

53 F. Auzel, Upconversion and Anti-Stokes Processes with f and d Ions in Solids, *Chem. Rev.*, 2004, **104**, 139–174.

54 L. Guerbous and O. Krachni, The 4f-5d luminescence transitions in cerium-doped LuF3, *J. Mod. Opt.*, 2006, **53**, 2043–2053.

55 S. Zazubovich, V. V Laguta, P. Machek, K. Kamada, A. Yoshikawa and M. Nikl, Effect of Li+ co-doping on the luminescence and defects creation processes in Gd3(Ga,Al)5O12:Ce scintillation crystals, *J. Lumin.*, 2022, **242**, 118548.

56 J. Wang, Y. Xie, Z. Zhang, J. Li, X. Chen, L. Zhang, R. Xu and X. Zhang, Photocatalytic degradation of organic dyes with Er3+:YAlO3/ZnO composite under solar light, *Sol. Energy Mater. Sol. Cells*, 2009, **93**, 355–361.

57 R. Xu, J. Li, J. Wang, X. Wang, B. Liu, B. Wang, X. Luan and X. Zhang, Photocatalytic degradation of organic dyes under solar light irradiation combined with Er3+:YAlO3/Fe- and Co-doped TiO2 coated composites, *Sol. Energy Mater. Sol. Cells*, 2010, **94**, 1157–1165.

58 W. Qin, D. Zhang, D. Zhao, L. Wang and K. Zheng, Near-infrared photocatalysis based on YF3:Yb3+, Tm3+/TiO2 core/shell nanoparticles, *Chem. Commun.*, 2010, **46**, 2304–2306.

59 J. Gao, X. Luan, J. Wang, B. Wang, K. Li, Y. Li, P. Kang and G. Han, Preparation of Er3+:YAlO3/Fe-doped TiO2-ZnO and its application in photocatalytic degradation of dyes under solar light irradiation, *Desalination*, 2011, **268**, 68–75.

60 L. Yin, J. Gao, J. Wang, X. Luan, P. Kang, Y. Li, K. Li and X. Zhang, Synthesis of Er 3+:Y 3Al 5O 12 and its effects on the solar light photocatalytic activity of TiO 2-ZrO 2 composite, *Res. Chem. Intermed.*, 2012, **38**, 523–536.

61 W. Wang, W. Huang, Y. Ni, C. Lu and Z. Xu, Different Upconversion Properties of β-NaYF4:Yb3+,Tm3+/Er3+ in Affecting the Near-Infrared-Driven Photocatalytic Activity of High-Reactive TiO2, *ACS Appl. Mater. Interfaces*, 2014, **6**, 340–348.

62 X. Guo, W. Song, C. Chen, W. Di and W. Qin, Near-infrared photocatalysis of β-NaYF4:Yb 3+,Tm3+@ZnO composites, *Phys. Chem. Chem. Phys.*, 2013, **15**, 14681–14688.

63 Y. Tang, W. Di, X. Zhai, R. Yang and W. Qin, NIR-responsive photocatalytic activity and mechanism of NaYF 4:Yb,Tm@TiO2 core-shell nanoparticles, *ACS Catal.*, 2013, **3**, 405–412.

64 Y. Zhang and Z. Hong, Synthesis of lanthanide-doped NaYF4@TiO2 core–shell composites with highly crystalline and tunable TiO2 shells under mild conditions and their upconversion-based photocatalysis, *Nanoscale*, 2013, **5**, 8930–8933.

65 J. Zhao, D. Jin, E. P. Schartner, Y. Lu, Y. Liu, A. V. Zvyagin, L. Zhang, J. M. Dawes, P. Xi, J. A. Piper, E. M. Goldys and T. M. Monro, Single-nanocrystal sensitivity achieved by enhanced upconversion luminescence, *Nat. Nanotechnol.*, 2013, **8**, 729–734.

66 L. Bai, W. Jiang, C. Gao, S. Zhong, L. Zhao, Z. Li and S. Bai, Facet engineered interface design of NaYF4:Yb,Tm upconversion nanocrystals on BiOCl nanoplates for enhanced near-infrared photocatalysis, *Nanoscale*, 2016, **8**, 19014–19024.

67 Z. Li, H. Cao, Z. Yin, X. Dong, J. Hao, Z. Song, Z. Yang, J. Qiu and Y. Li, Photon upconversion in Bi3Ti2O8F:Yb3+, Er3+ nanoplates for enhanced near-infrared light harvesting and their application in wastewater purification, *J. Environ. Chem. Eng.*, 2025, **13**, 115661.

68 Z. Hong, F. Lai, W. You, B. Wang and J. Huang, Near-infrared responsive upconversion of lanthanide doped Bi-based glass ceramics for norfloxacin degradation, *Ceram. Int.*, 2025, **51**, 8353–8361.

69 L. Wang, C. Xia, T. Yang, H. Wang, N. Liu and C. Liang, Spindle-like porous N-doped TiO2 encapsulated (Ca,Y) F2:Yb3+,Tm3+ as the efficient photocatalyst near-infrared range, *Nanotechnology*, 2020, **31**, 025601.

70 P. O'Callaghan, A. Jarosz-Duda, J. Kuncewicz, K. Dzierżęga and W. Macyk, Upconverting particles in near-infrared light-induced TiO2 photocatalysis: towards the optimal architecture of upconverter/photocatalyst systems, *RSC Adv.*, 2024, **14**, 36930–36936.

71 Z. Ma, X. Song, Y. Lu, F. Zhu, Y. Xie, L. Zhao, Z. Yang and J. Zhang, Joint Electrons and Photons Transfer from Dual-Functional WO3:Yb,Er to Zn0.5Cd0.5S for Efficient H2 Evolution, *Adv. Energy Mater.*, 2025, **15**, 2403307.

72 K. Feng, Z. Cai, D. Huang, L. Li, K. Wang, Y. Li, C. Wang, J. Song, L. Zhao, W. Wei and F. Jiang, Near-infrared-driven water splitting for hydrogen evolution using a Cu2ZnSnS4-based photocathode by the application of

upconversion nanoparticles, *Sustainable Energy Fuels*, 2020, **4**, 2669–2674.

73 X. Gao, N. Yang, J. Feng, J. Liao, S. Hou, X. Ma, D. Su, X. Yu, Z. Yang, J. Safaei, D. Wang and G. Wang, Defect and interface control on graphitic carbon nitrides/upconversion nanocrystals for enhanced solar hydrogen production, *Natl. Sci. Open*, 2023, **2**, DOI: 10.1360/nso/20220037.

74 J.-W. Lee, K.-H. Cho, J.-S. Yoon and Y.-M. Sung, Enhanced IR-driven photoelectrochemical responses of CdSe/ZnO heterostructures by up-conversion UV/visible light irradiation, *Nanoscale*, 2020, **12**, 8525–8535.

75 G. Murali, S. V Prabhakar Vattikuti, Y. K. Kshetri, H. Lee, J. K. R. Modigunta, Ch. Seshendra Reddy, S. Park, S. Lee, B. Poornaprakash, H. Lee, Y. H. Park, J. Lee, S. Y. Park and I. In, Near-infrared-activated Z-scheme NaYF4:Yb/Tm@Ag3PO4/Ag@g-C3N4 photocatalyst for enhanced H2 evolution under simulated solar light irradiation, *Chem. Eng. J.*, 2021, **421**, 129687.

76 J. Méndez-Ramos, M. E. Borges, S. Torres-García, M. Medina-Alayón, P. Acosta-Mora, J. del-Castillo, A. Menéndez-Velázquez, A. B. García-Delgado, C. B. Mullins and P. Esparza, "There is plenty of energy at the bottom": A spectral conversion approach for upconversion-powered water-splitting PEC cell, *J. Power Sources*, 2025, **625**, 235668.

77 J. Méndez-Ramos, J. C. Ruiz-Morales, P. Acosta-Mora, J. Del-Castillo and A. C. Yanes, Rare-earth doped nano-glass-ceramics for extending spectral response of water-splitting semiconductor electrodes by high intense UV-blue up-conversion: Turning the sun into blue, *J. Power Sources*, 2013, **238**, 313–317.

78 W. Gao, Y. Wu and G. Lu, 980 nm NIR light driven overall water splitting over a combined CdS-RGO-NaYF4-Yb3+/Er3+ photocatalyst, *Catal. Sci. Technol.*, 2020, **10**, 2389–2397.

79 M. Zhang, Y. Lin, T. J. Mullen, W. F. Lin, L. D. Sun, C. H. Yan, T. E. Patten, D. Wang and G. Y. Liu, Improving hematites solar water splitting efficiency by incorporating rare-earth upconversion nanomaterials, *J. Phys. Chem. Lett.*, 2012, **3**, 3188–3192.

80 C. K. Chen, H. M. Chen, C. J. Chen and R. S. Liu, Plasmon-enhanced near-infrared-active materials in photoelectrochemical water splitting, *Chem. Commun.*, 2013, **49**, 7917–7919.

81 A. K. Verma, P. Tripathi, H. Kumar, P. Singh, A. S. K. Sinha and S. Singh, Engineering Upconversion Semiconductor Nanostructures: Unravelling the Morphology–Performance Relationship for Photocatalytic Hydrogen Generation, *ACS Appl. Energy Mater.*, 2025, **8**, 11977–11987.

82 Z. Wang, M. Wu, X. Cui, F. Ge, P. Xiao, M. Li and H. Fu, Triplet–Triplet Annihilation Upconversion with Large Anti-Stokes Shift, *ACS Nano*, 2025, **19**, 25596–25616.

83 L. Huang and G. Han, Triplet–triplet annihilation photon upconversion-mediated photochemical reactions, *Nat. Rev. Chem.*, 2024, **8**, 238–255.

84 C. Ye, J. Wang, X. Wang, P. Ding, Z. Liang and X. Tao, A new medium for triplet–triplet annihilated upconversion and photocatalytic application, *Phys. Chem. Chem. Phys.*, 2016, **18**, 3430–3437.

85 S. Chandrasekaran, Y.-L. T. Ngo, L. Sui, E. J. Kim, D. K. Dang, J. S. Chung and S. H. Hur, Highly enhanced visible light water splitting of CdS by green to blue upconversion, *Dalton Trans.*, 2017, **46**, 13912–13919.

86 D. Choi, S. K. Nam, K. Kim and J. H. Moon, Enhanced Photoelectrochemical Water Splitting through Bismuth Vanadate with a Photon Upconversion Luminescent Reflector, *Angew. Chem.*, 2019, **131**, 6965–6969.

87 J. Fang, Y. Chen, W. Wang, L. Fang, C. Lu, C. Zhu, J. Kou, Y. Ni and Z. Xu, Highly efficient photocatalytic hydrogen generation of g-C3N4-CdS sheets based on plasmon-enhanced triplet–triplet annihilation upconversion, *Appl. Catal., B*, 2019, **258**, 117762.

88 M. Barawi, F. Fresno, R. Pérez-Ruiz and V. A. de la Peña O'Shea, Photoelectrochemical Hydrogen Evolution Driven by Visible-to-Ultraviolet Photon Upconversion, *ACS Appl. Energy Mater.*, 2019, **2**, 207–211.

89 T. Yu, Y. Liu, Y. Zeng, J. Chen, G. Yang and Y. Li, Triplet–Triplet Annihilation Upconversion for Photocatalytic Hydrogen Evolution, *Chem. - Eur. J.*, 2019, **25**, 16270–16276.

90 Y. Kageshima, S. Tateyama, F. Kishimoto, K. Teshima, K. Domen and H. Nishikiori, Photocatalytic oxygen evolution triggered by photon upconverted emission based on triplet–triplet annihilation, *Phys. Chem. Chem. Phys.*, 2021, **23**, 5673–5679.

91 S. Liu, H. Liu, Y. Hu, C. Zhao, H. Huang, G. Yu, Z. Li, Z. Liu, Y. Chen and X. Li, Boosting photocatalytic hydrogen evolution via triplet–triplet annihilation upconversion, *Chem. Eng. J.*, 2023, **452**, 139203.

92 Y. Magazov, V. Kudryashov, K. Moldabekov, M. Amze, A. Nurmanova, A. Aliyev and N. Nuraje, Copper oxide coupled with photon upconversion for solar water splitting, *Commun. Mater.*, 2024, **5**, 126.

93 X. Lin, Y. Hao, Y. Gong, P. Zhou, D. Ma, Z. Liu, Y. Sun, H. Sun, Y. Chen, S. Jia, W. Li, C. Guo, Y. Zhou, P. Huo, Y. Yan, W. Ma, S. Yuan and J. Zhao, Solar overall water-splitting by a spin-hybrid all-organic semiconductor, *Nat. Commun.*, 2024, **15**, 5047.

94 P. Venkatesan, J.-Y. Lin, D. Roy, P. Aloni, Z.-F. Lin and R.-A. Doong, Enhanced solar-driven photoelectrocatalytic water treatment and hydrogen evolution with triplet-triplet annihilation upconversion with Mo-doped BiVO4 nanocomposite films, *Appl. Catal. B Environ. Energy*, 2025, **365**, 124913.

95 X. Chen, Z. Xian, S. Gao, L. Bai, S. Liang, H. Tian, C. Wang and C. Gu, Mechanistic insights into surface catalytic oxidation of fluoroquinolone antibiotics on sediment mackinawite, *Water Res.*, 2023, **232**, 119651.

96 P. Venkatesan, J. Y. Lin, D. Roy, P. Aloni, Z. F. Lin and R. A. Doong, Enhanced solar-driven photoelectrocatalytic water treatment and hydrogen evolution with triplet-triplet annihilation upconversion with Mo-doped BiVO4 nanocomposite films, *Appl. Catal., B*, 2025, **365**, 124913.

97 P. Bharmoria, S. Hisamitsu, H. Nagatomi, T. Ogawa, M. Morikawa, N. Yanai and N. Kimizuka, Simple and Versatile Platform for Air-Tolerant Photon Upconverting Hydrogels by Biopolymer–Surfactant–Chromophore Co-assembly, *J. Am. Chem. Soc.*, 2018, **140**, 10848–10855.

98 H. Kim, S. Weon, H. Kang, A. L. Hagstrom, O. S. Kwon, Y.-S. Lee, W. Choi and J.-H. Kim, Plasmon-Enhanced Sub-Bandgap Photocatalysis via Triplet–Triplet Annihilation Upconversion for Volatile Organic Compound Degradation, *Environ. Sci. Technol.*, 2016, **50**, 11184–11192.

99 J. Fang, W. Wang, C. Zhu, L. Fang, J. Jin, Y. Ni, C. Lu and Z. Xu, CdS/Pt photocatalytic activity boosted by high-energetic photons based on efficient triplet–triplet annihilation upconversion, *Appl. Catal., B*, 2017, **217**, 100–107.

100 J. Fang, C. Zhou, Y. Chen, L. Fang, W. Wang, C. Zhu, Y. Ni and C. Lu, Efficient Photocatalysis of Composite Films Based on Plasmon-Enhanced Triplet–Triplet Annihilation, *ACS Appl. Mater. Interfaces*, 2020, **12**, 717–726.

101 J. Fang, C. Zhu, Y. Ni, C. Lu and Z. Xu, Double local electromagnetic fields collaboratively enhanced triplet–triplet annihilation upconversion for efficient photocatalysis, *Catal. Sci. Technol.*, 2023, **13**, 2151–2159.

102 H. Cho, S. E. Seo, O. S. Kwon and H. Kim, Photonic crystal-assisted sub-bandgap photocatalysis via triplet-triplet annihilation upconversion for the degradation of environmental organic pollutants, *J. Hazard. Mater.*, 2024, **477**, 135208.

103 J. Liu, T. Sui, Y. Zhang, H. Bian, Y. Lu and C. Zhu, Mechanistic and Kinetic Insights into Hydroxyl Radical-Mediated Tetracycline Transformation in Photocatalytic Oxidation Processes, *Catalysts*, 2025, **15**, DOI: 10.3390/catal15050420.

104 E. L. Cates, S. L. Chinnapongse, J.-H. Kim and J.-H. Kim, Engineering Light: Advances in Wavelength Conversion Materials for Energy and Environmental Technologies, *Environ. Sci. Technol.*, 2012, **46**, 12316–12328.

105 M. Haase and H. Schäfer, Upconverting Nanoparticles, *Angew. Chem., Int. Ed.*, 2011, **50**, 5808–5829.

106 X. Cheng, J. Zhou, J. Yue, Y. Wei, C. Gao, X. Xie and L. Huang, Recent Development in Sensitizers for Lanthanide-Doped Upconversion Luminescence, *Chem. Rev.*, 2022, **122**, 15998–16050.

107 B. S. Richards, D. Hudry, D. Busko, A. Turshatov and I. A. Howard, Photon Upconversion for Photovoltaics and Photocatalysis: A Critical Review, *Chem. Rev.*, 2021, **121**, 9165–9195.

108 M. Uji, T. J. B. Zähringer, C. Kerzig and N. Yanai, Visible-to-UV Photon Upconversion: Recent Progress in New Materials and Applications, *Angew. Chem., Int. Ed.*, 2023, **62**, e202301506.

109 S. P. Sahu, S. L. Cates, H.-I. Kim, J.-H. Kim and E. L. Cates, The Myth of Visible Light Photocatalysis Using Lanthanide Upconversion Materials, *Environ. Sci. Technol.*, 2018, **52**, 2973–2980.